# Quarterly Technical Report

## Growth, Characterization and Device Development in Monocrystalline Diamond Films

Supported under Grant #N00014-93-I-0437
Office of the Chief of Naval Research
Report for the period 4/1/97–6/30/97

R. F. Davis, R. J. Nemanich* and Z. Sitar
P. Baumann, W. Liu, R. Schlesser, C. A. Wolden, and P. C. Yang
North Carolina State University
c/o Materials Science and Engineering Department
*Department of Physics
Box 7907
Raleigh, NC 27695



June, 1997

# REPORT DOCUMENTATION PAGE

Form Approved
OMB No. 0704-0188



| 1. AGENCY USE ONLY *(Leave blank)* | 2. REPORT DATE | 3. REPORT TYPE AND DATES COVERED |
|---|---|---|
| | June, 1997 | Quarterly Technical 4/1/97-6/30/97 |

**4. TITLE AND SUBTITLE**

Growth, Characterization and Device Development in Monocrystalline Diamond Films

**5. FUNDING NUMBERS**

s400003srr14
1114SS
N00179
N66005
4B855

**6. AUTHOR(S)**

R. F. Davis, R. J. Nemanich, and Z. Sitar

**7. PERFORMING ORGANIZATION NAME(S) AND ADDRESS(ES)**

North Carolina State University
Hillsborough Street
Raleigh, NC 27695

**8. PERFORMING ORGANIZATION REPORT NUMBER**

N00014-93-I-0437

**9. SPONSORING/MONITORING AGENCY NAMES(S) AND ADDRESS(ES)**

Sponsoring: ONR, Code 312, 800 N. Quincy, Arlington, VA 22217-5660
Monitoring: Admin. Contracting Officer, Office of Naval Research
Atlanta Regional Office
100 Alabama Street, Suite 4R15
Atlanta, GA 30303

**10. SPONSORING/MONITORING AGENCY REPORT NUMBER**

**11. SUPPLEMENTARY NOTES**

**12a. DISTRIBUTION/AVAILABILITY STATEMENT**

Approved for Public Release; Distribution Unlimited

**12b. DISTRIBUTION CODE**

**13. ABSTRACT** ***(Maximum 200 words)***

Highly oriented diamond has been grown on (100) Ni substrates by the hot filament chemical vapor deposition method. Epitaxial nuclei were obtained by diamond powder seeding and a subsequent high-temperature annealing process. Real time, *in situ* laser reflectometry was developed to monitor changes in surface morphology observed during the high temperature annealing since the timing of the process was crucial for the achievement of a high degree of orientation and a high density of diamond nuclei. Characteristic features observed in the intensities of reflected and scattered light were interpreted by comparison with scanning electron micrographs of the samples quenched at sequential stages of the process. It was concluded that the scattered light signal can be effectively used as a process steering parameter. Auger spectroscopy showed that up to 6 at% of the C was dissolved in the Ni surface layer. The investigation of interfacial microstructures and phases involved by transmission electron microscopy revealed the formation of $Ni_4C$ already in the early stages of nucleation. This phase was manifested as coherent precipitates and is believed to have been the precursor for diamond nucleation. Perfectly epitaxial diamond was grown by this process. The epitaxial relationship was determined by cross-sectional transmission electron microscopy and selected area diffraction analysis. Ultra photo spectroscopy and field emission measurements were employed to correlate the electron affinity and Schottky barrier height of Cu films on type IIb (p-type) diamond (100), (111) and (110) surfaces. The latter were correlated with the effective electron affinity of the samples.

**14. SUBJECT TERMS**

diamond, Ni, chemical vapor deposition, seeding, laser reflectometry, Auger spectroscopy, interfacial microstructures, $Ni_4C$, field emission, transmission electron microscopy, ultra photoelectron spectroscopy, electron affinity

**15. NUMBER OF PAGES**

41

**16. PRICE CODE**

| 17. SECURITY CLASSIFICATION OF REPORT | 18. SECURITY CLASSIFICATION OF THIS PAGE | 19. SECURITY CLASSIFICATION OF ABSTRACT | 20. LIMITATION OF ABSTRACT |
|---|---|---|---|
| UNCLAS | UNCLAS | UNCLAS | SAR |

# Table of Contents

# I. Introduction

Diamond as a semiconductor in high-frequency, high-power transistors has unique advantages and disadvantages. Two advantages of diamond over other semiconductors used for these devices are its high thermal conductivity and high electric-field breakdown. The high thermal conductivity allows for higher power dissipation over similar devices made in Si or GaAs, and the higher electric field breakdown makes possible the production of substantially higher power, higher frequency devices than can be made with other commonly-used semiconductors.

In general, the use of bulk crystals severely limits the potential semiconductor applications of diamond. Among several problems typical for this approach are the difficulty of doping the bulk crystals, device integration problems, high cost and low area of such substrates. In principal, these problems can be alleviated via the availability of chemically vapor deposited (CVD) diamond films. Recent studies have shown that CVD diamond films have thermally activated conductivity with activation energies similar to crystalline diamonds with comparable doping levels. Acceptor doping via the gas phase is also possible during activated CVD growth by the addition of diborane to the primary gas stream.

The recently developed activated CVD methods have made feasible the growth of polycrystalline diamond thin films on many non-diamond substrates and the growth of single crystal thin films on diamond substrates. More specifically, single crystal epitaxial films have been grown on the {100} faces of natural and high pressure/high temperature synthetic crystals. Crystallographic perfection of these homoepitaxial films is comparable to that of natural diamond crystals. However, routes to the achievement of rapid nucleation on foreign substrates and heteroepitaxy on one or more of these substrates has proven more difficult to achieve. This area of study has been a principal focus of the research of this contract.

At present, the feasibility of diamond electronics has been demonstrated with several simple experimental devices, while the development of a true diamond-based semiconductor materials technology has several barriers which a host of investigators are struggling to surmount. It is in this latter regime of investigation that the research described in this report has and continues to address.

In this reporting period, (1) highly oriented diamond has been grown on (100) Ni substrates by the hot filament chemical vapor deposition method from epitaxial nuclei obtained by diamond powder seeding and subsequent high-temperature annealing, and (2) copper-diamond (100) (111) (110) interfaces have been characterized for their electron affinity and Schottky barrier. The following section is self-contained in that it presents an introduction, the experimental procedures, results and discussion, summary and indications of future research for the given research thrust.

## II. Heteroepitaxial Nucleation of Diamond on Nickel

### A. Introduction

The heteroepitaxy of diamond films on nickel substrates by chemical vapor deposition (CVD) has been subject of intensive research both experimentally and theoretically [1-3]. Nickel is one of the few materials that has a close lattice match with diamond (a=3.52Å for Ni vs. a=3.56Å for diamond). It has been known for decades that Ni is an effective solvent-catalyst metal for diamond crystallization under high pressure and high temperature (HPHT) conditions [4]. HPHT synthetic diamond often contains crystalline nickel inclusions. Early x-ray diffraction (XRD) studies of this material showed additional reflections corresponding to a lattice spacing close to that of diamond (200) planes. It was found that they arose from a Ni-rich face-centered cubic phase which was identified as $Ni_4C$ carbide [5].

However, nickel's high solubility for carbon and its strong catalytic effect on hydrocarbon decomposition at low pressures have prevented CVD diamond nucleation on the Ni surface without the deposition of an intermediate graphite layer [6]. The graphite interlayer generally formed immediately after a Ni substrate was placed into a methane-hydrogen CVD environment. Belton and Schmieg [6] reported on a study of filament-assisted diamond film growth on single crystalline Ni (100) substrates. Graphite islands with poor azimuthal orientation were observed after two minutes of growth. At longer times, the graphite became disordered. Even though diamond eventually nucleated and grew on the graphitic interlayer, this precluded the possibility of an orientational relationship between the diamond film and the Ni substrate.

Sato *et al.* [7] reported that both (111) and (100) oriented diamond nuclei could be grown on Ni substrates, but the overall percentage of oriented nuclei was rather low. Yang *et al.* [1-3] reported on a novel hot filament CVD (HFCVD) process for nucleation of oriented diamond films on both single crystal and polycrystalline nickel substrates. Tachibana [8] reported on highly oriented (111) diamond grown on Pt substrates using similar conditions. In both cases, it appeared that carbon first formed an intermediate phase with metal, which subsequently served as a precursor for diamond nucleation.

Although the growth process on nickel is very successful, there are still many questions associated with the mechanism of the oriented diamond nucleation. The success of this process depends primarily on the nucleation step. In order to gain control over the conditions leading to highly oriented diamond, we designed and commissioned an optical system which enabled optimization of the nucleation step and reproducibility of the whole process from run to run. We have ample evidence that a molten Ni-C-H surface eutectic plays a crucial role in the nucleation process. Formation of $Ni_4C$ in the early stages of the process, before the formation of diamond, suggests that diamond does not nucleate directly on the Ni metal but rather on its

carbide. The same carbide phase remains present at the diamond nickel interface also after the growth.

This report first describes a three-step growth process and explains how the observed changes in the surface morphology were used for the control of the nucleation step. A complete analysis of the process is given based on results obtained from structural and chemical analyses of the samples obtained at different stages. Based on these observations, a nucleation mechanism for diamond on nickel is proposed.

B. Experimental Procedures

All experiments were carried out in a hot-filament CVD (HFCVD) system. The growth chamber was modified to allow *in situ* optical measurements of reflective and scattering properties of the sample surface. Figure 1 shows the set-up of the optical monitoring system. A He-Ne laser ($\lambda$=633nm) illuminated the sample under normal incidence. A prism was used as a semi-transparent beam splitter which directed the reflected beam from the sample to a photodiode (D1). Light scattered at the sample's surface was detected by a second photodiode (D2) under an angle of 5° from the surface normal. The view field of D2 was defined by a set of apertures. In order to discriminate between the probe beam and the intense light of the filament used for dissociation of $H_2$, each detector was equipped with an optical interference filter. Furthermore, the incident laser beam was mechanically chopped ($\upsilon$= 500 Hz). The relatively strong reflected signal was processed by an AC to DC RMS converter, which

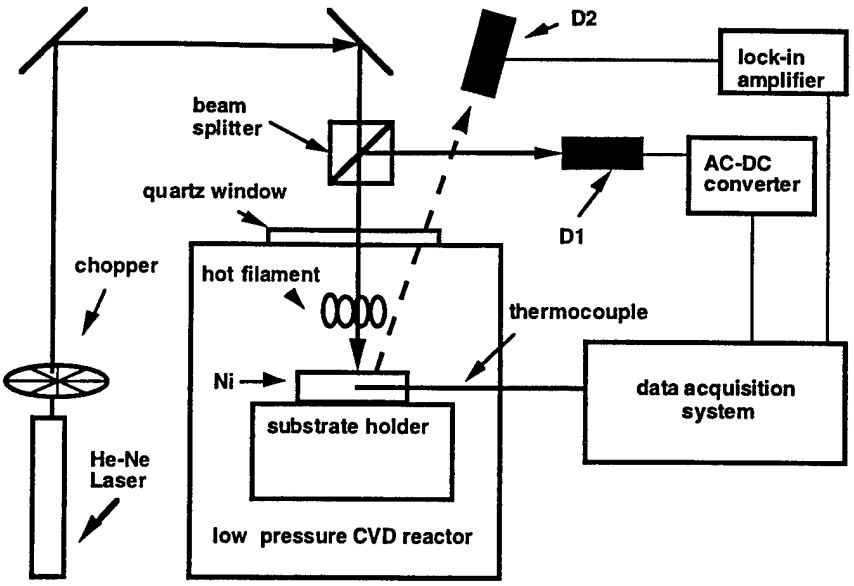


Figure 1. Schematic of the hot filament reactor equipped with the optical control system.

suppressed the constant filament light contribution. A phase-sensitive lock-in amplifier was used to detect the weaker scattering signal. The substrate temperature was measured by a type C thermocouple imbedded ~100 μm beneath the substrate surface. All optical and temperature signals were recorded simultaneously by a Macintosh-based data acquisition system.

One mm thick pieces of (100) single crystalline Ni were used as substrates. A multi-step process involving seeding with diamond powder and high temperature annealing was used to obtain oriented nucleation. A suspension of 0.5 μm diamond powder in acetone was used for the seeding. Samples were simply immersed into suspension and allowed to dry. Following the seeding, samples were introduced into the system and substrate temperature was quickly raised to about 1050°C in the presence of atomic hydrogen. After a short hold at these conditions, the substrate temperature was lowered to about 900°C and 0.5% $CH_4$ was introduced to begin diamond growth. In order to observe changes on the seeded surface as well as deeper in the sample, samples were quenched at different stages of the process and examined by scanning electron microscopy (SEM), transmission electron microscopy (TEM), and Auger spectroscopy. The observed surface topography was correlated with the changes in scattered and reflected light intensities which were recorded throughout the experiments.

Plan-view and cross-sectional TEM samples were prepared from samples which underwent different annealing times and from samples after the completed growth. The plan-view sample was prepared by standard methods [9]. For the cross-sectional samples, difficulties arose due to the extreme differences in hardness between diamond and nickel. These samples were prepared using a focused ion beam technique. The microstructural studies were performed with a TOPCON EM-002B operated at 200 kV.

C. Results and Discussion

During the annealing stage, the seeded surface underwent significant changes in the morphology which were manifested in changes in surface reflectivity. Figure 2 shows typical changes in the substrate temperature and the intensities of reflected and scattered light during this process. Initially, the reflected light intensity was weak due to considerable scattering losses on the diamond seeds. After the substrate temperature was increased to 1050°C, a rapid increase in the reflected light signal was observed, accompanied by a transient peak in the scattered light intensity. At the high temperature, the reflected light intensity saturated while the scattered light signal decreased. The typical changes in the optical signals (i.e., the rapid increase in reflectivity, accompanied by a transient peak in scattered intensity) were found to be reproducible from run to run and were, therefore, well suited as monitoring and control signals.

In order to correlate the observed optical signals with surface features, samples were quenched at four different times ($t_1$,..,$t_4$) of the process, as indicated in Fig. 2, and analyzed by

SEM. Figure 3($t_1$) shows the surface after diamond seeding and before annealing. Evidently, the seeding procedure provided a uniform coverage across the substrate. At time $t_2$, as the reflected light intensity began to increase, the layer of diamond seeds was no longer continuous and diamond particles became nonuniform in size. A large fraction of the diamond seeds either dissolved into the substrate or were etched away by the atomic hydrogen. The dissolution theory is supported by the fact that the seeds in an intimate contact with the nickel surface were affected more than the seeds lying on the top of other diamond particles. Furthermore, the rate at which the seeds were disappearing (approximately 1 μm/min) could not be explained by the very slow etch rates of diamond in atomic hydrogen environment [10]. The rapid dissolution rate indicated the presence of a surface molten layer. A true solid-solid reaction would be expected to be much slower since the diffusion coefficient of C in solid Ni is several orders of magnitude smaller than that in a molten state [11]. At the time $t_3$, when the scattered light was most intense, the population of the diamond seeds was greatly reduced and the size became again more uniform, ranging from 100 to 200 nm. The observed particle size was consistent

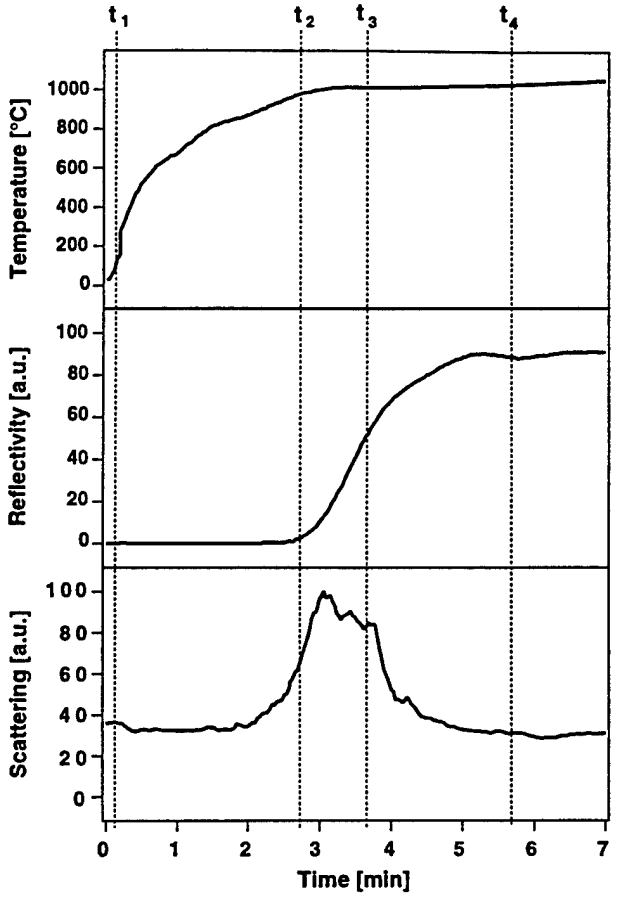


Figure 2. Changes in temperature, and reflected and scattered light intensities during the annealing step. At times $t_1$...$t_4$, samples were quenched and examined by SEM (Fig. 3).

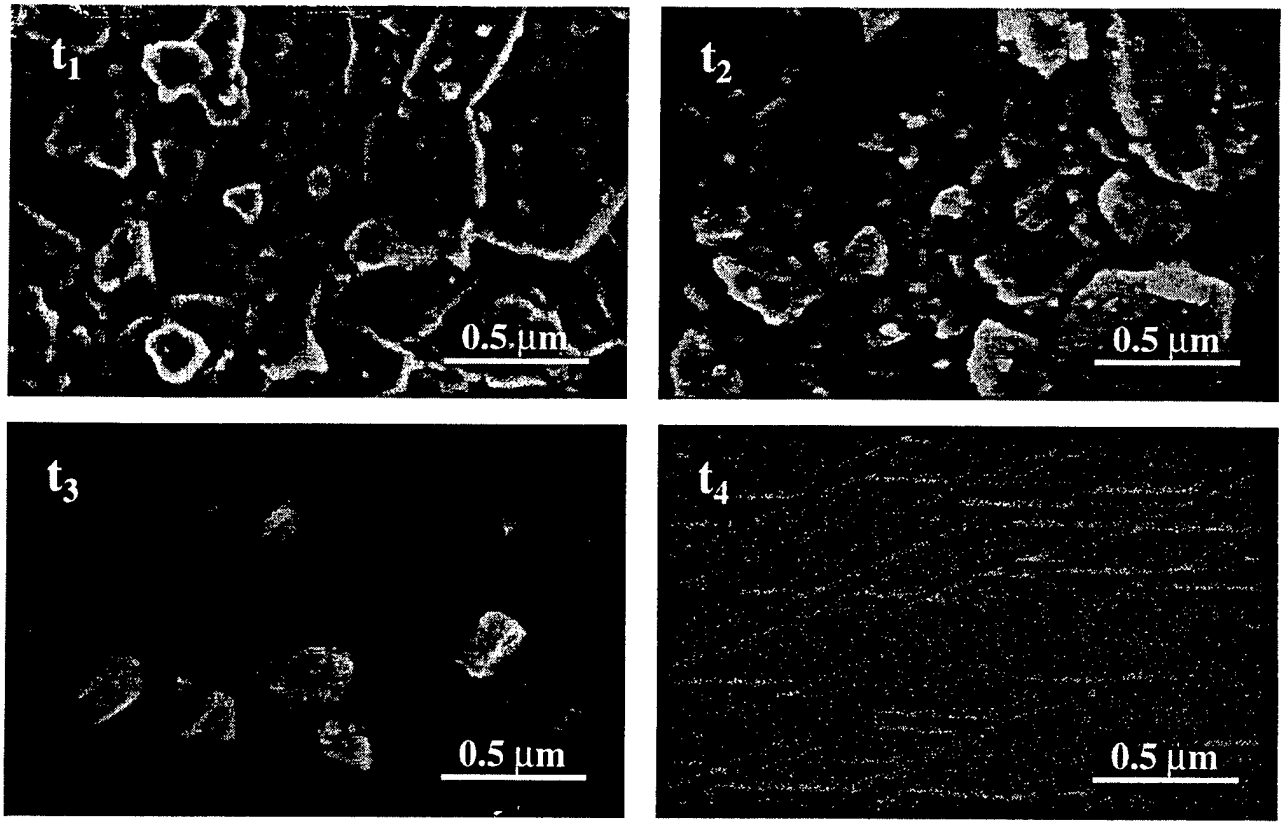


Figure 3. SEM micrographs of samples quenched at different times of the annealing process. Figures $t_1$...$t_4$ correspond to times indicated in Fig. 2.

with the expected maximum in the size dependent optical scattering efficiency. At time $t_4$, all diamond seeds had disappeared from the surface and upon cooling an ordered crystalline surface morphology was obtained as shown in Fig. 3($t_4$). At this point, a mirror like metallic surface was observed, the reflected light intensity saturated while the scattered light intensity decreased.

In order to achieve a high degree of oriented diamond nucleation, the primary, random diamond seeds must be completely reacted with the nickel substrate. Any remainders of original seeds would result in randomly oriented diamond films. The fact that oriented diamond nucleation on nickel does not require primary diamond particles was further supported by the graphite seeding which produced similar end results. On the other hand, it is critical to stop the annealing process immediately after all the seeds had dissolved. Further annealing would diminish carbon concentration at the surface by diffusion into the substrate and subsequently lower the nucleation density. Thus, the exact timing of the annealing process was essential for high density of oriented particles. The disappearance of the particles from the surface was indicated by a rapid decrease in the scattered light intensity after it had reached a peak value. This signal was found to be a more sensitive and reliable indicator of the surface changes than

the reflected light signal. Based on its sensitivity to changes in surface morphology, the scattered light signal was chosen as the indicator of the time to change the experimental conditions from the annealing stage to the normal growth stage. After the scattered light intensity had dropped, the substrate temperature was lowered from 1050°C to 950°C and 0.5% $CH_4$ in $H_2$ was introduced to initiate the growth. A steady increase in the scattered light and decrease in reflected light signals were observed during the growth of diamond.

The recrystallized sample obtained at $t_4$ was used for carbon concentration studies by Auger spectroscopy. To gain the information on carbon concentration at the surface as well as deep in the bulk a shallow, 0.85° wedge was polished on the surface of the sample and an Auger line scan was performed. The schematic of the wedge-polished sample is shown in the inset of Fig. 4. The scan from A to B measured the surface, while the region from B to D probed the interior of the nickel substrate. Three distinct regions of carbon concentration along this path can be observed in Fig. 4: first, the recrystallized surface (A to B) was characterized by a constant, high level of carbon which amounted to 6 at%. The carbon concentration then fell off in a short transition region (B to C), before leveling out at a constant value of 3 at% in the bulk (C to D). It is important to note that the carbon level in the Ni substrate before the processing was below the detection limit of the instrument. From the wedge angle, the depth of the transition region was calculated to be less than 1 μm. The quantification of the carbon concentration was conducted by using the peak to peak value from the survey scan data and the sensitivity factors for each element. The error in the absolute values was estimated to be about

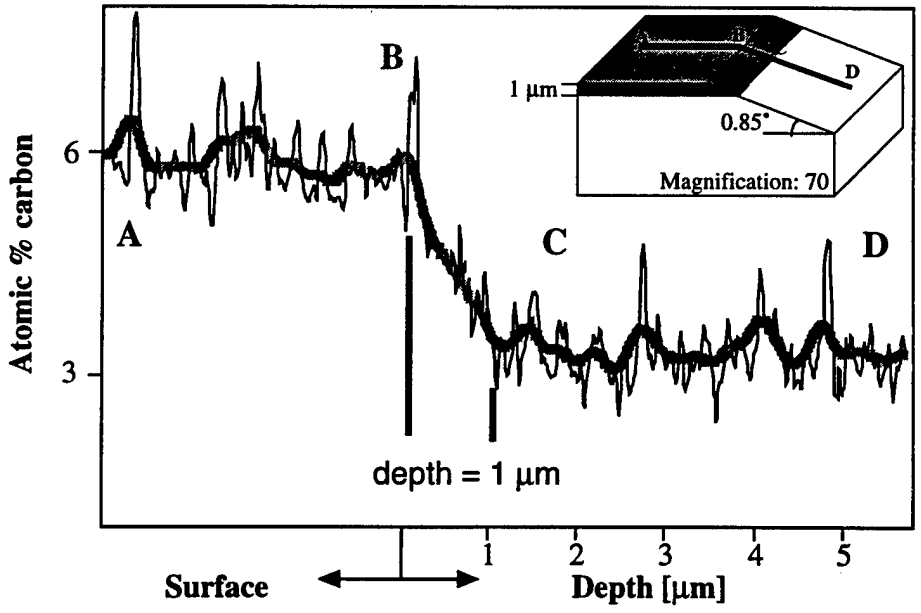


Figure 4. Carbon concentration as a function of position on the wedge polished sample shown in the inset.

30%. Despite the uncertainty, the obtained values are in good correspondence with the Ni-C equilibrium phase diagram. The 3 at% carbon measured in the bulk is the uppermost limit of the solid solubility of C in Ni, as obtained from the equilibrium Ni-C phase diagram, while the 6 at% of carbon in Ni at the surface is close to the eutectic composition of 8 at% [12]. The supersaturation of a thin surface layer with carbon and a constant, saturated value in the bulk also indicated the presence of a surface molten region. Since the reaction took place only in presence of atomic hydrogen, we suspect that the molten layer was a Ni-C-H eutectic.

In order to obtain information on structural relationships and possible formation of intermediate phases, extensive TEM analysis was performed. The two main questions to be answered were: In what form is carbon in nickel during and at the end of the annealing step and what is the interfacial relationship between nickel and oriented diamond after the growth?

Figure 5 shows a cross-section TEM image of a sample quenched after the scattered light intensity had peaked, corresponding to $t_3$ in Fig. 2. A polycrystalline, approximately 3000 Å thick structure was observed near the surface. The selected area diffraction (SAD) patterns taken from this structure and the substrate beneath it are shown as the insets of Fig. 5. Continuous diffraction rings indicative of a finely grained randomly oriented structure were observed close to the surface, while a crystalline Ni diffraction pattern superimposed on the ring pattern was obtained from the interfacial region between the top polycrystalline layer and the substrate. The polycrystalline rings were attributed to a mixture of nickel and $Ni_4C$. Although diamond has a similar lattice parameter, its sole presence could be excluded due to the

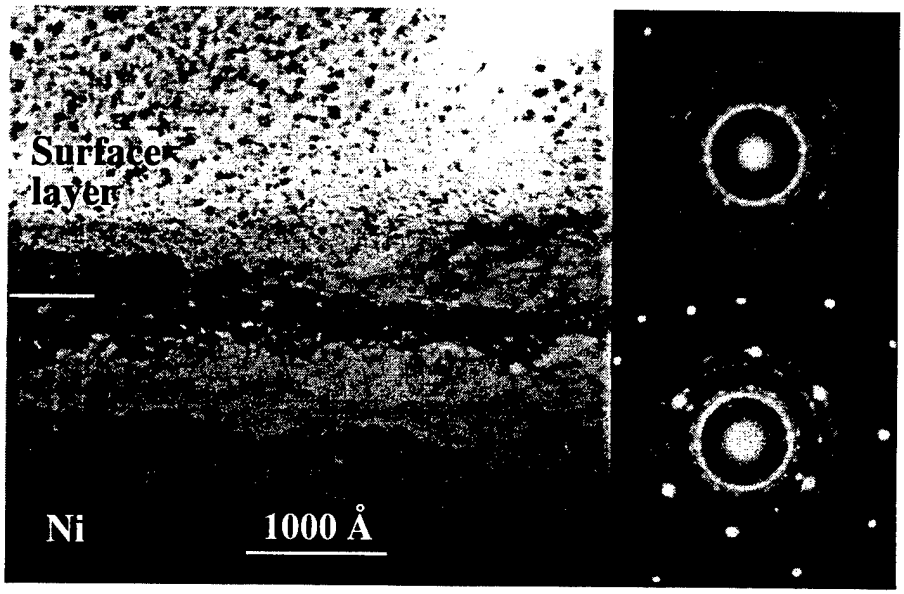


Figure 5. TEM image of a rapidly quenched sample, $t_3$, showing the original single crystal nickel and a finely-grained polycrystalline structure at the surface.

observed (200) diffraction ring. The formation of a polycrystalline layer on a single crystal substrate after the high temperature annealing and rapid quenching provided a strong indication of surface melting. A solid state diffusion process could not have accounted for the formation of the observed fine-grained polycrystalline structure near the surface. TEM investigation of a plan view specimen obtained from a sample at the end of the annealing stage, $t_4$ in Fig. 2, revealed round, coherent inclusions in otherwise perfectly crystalline nickel lattice, as shown in Fig. 6a. The inclusions were uniform in size and distributed throughout the specimen. They were about 50 nm in diameter and their planar density was estimated to be ~$10^8$ $cm^{-2}$. Contrast with the surrounding nickel lattice indicated that the average atomic mass of these inclusions was less than that of nickel. Figure 6b shows a SAD pattern originating from one of these inclusions and the surrounding Ni lattice. In addition to Ni diffraction spots, additional reflections (double spots indicated by arrows), which were perfectly oriented with the nickel pattern but corresponded to a material with a slightly larger lattice, were observed. The observed new phase should be either a carbide or diamond, which both have a slightly larger lattice parameter than nickel. Due to unsatisfied diffraction selection rules for the diamond lattice, the presence of diamond does not seem to be very likely and based on careful calculations we believe that the observed phase is $Ni_4C$.

After seven hours of diamond growth, the diamond particles showed very well developed facets and were on the average about 3 μm in size. They were well oriented with respect to each other and uniformly distributed across the sample, as observed by SEM. In order to study the orientation of diamond particles with respect to nickel substrate, a cross-section TEM sample was prepared by the focused ion beam technique. The TEM image of this sample, displayed in Fig. 7, shows three distinct regions: nickel substrate in the bottom part of the image, two well defined, faceted diamond particles in the middle, and a platinum protective layer on the top. The Pt layer was evaporated onto the sample to prevent the erosion of the

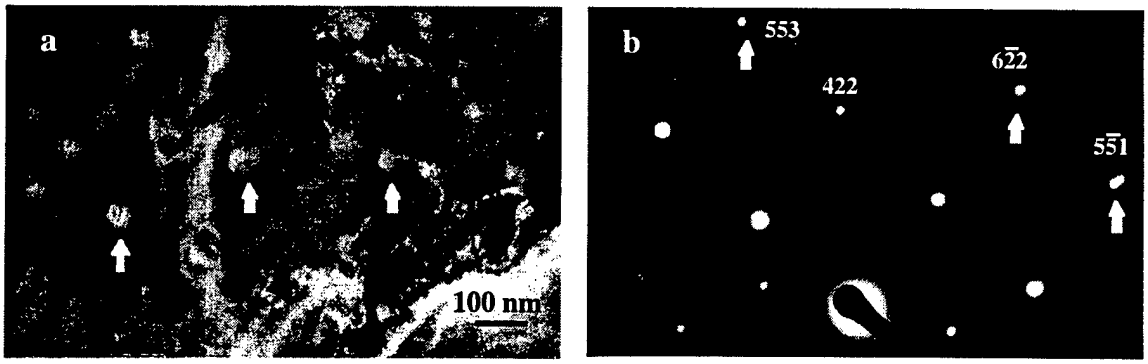


Figure 6. Plan view TEM image obtained after the annealing step (a) and corresponding SAD pattern (b). Arrows indicate the precipitates and double spots in (a) and (b), respectively.

surface by the impinging ions during the sample preparation. The narrow white regions between the Pt overlayer and underlying sample and under the edges of diamond particles occurred due to the delamination and nonconformal deposition of Pt and are not inherent to our diamond deposition process. A perusal of the surface and interfacial regions revealed a peak-to-valley roughness exceeding 1 μm. This is very much surprising since the Ni substrates underwent a final polish with 0.05 μm alumina. Apparently the surface roughened either during the high temperature annealing step, due to surface melting, or as a result of the stress produced by the growing diamond particles. It is also noteworthy that the diamond-nickel interface is not flat but rather strongly faceted. The facets observed at the interface are geometrically related to those observed on the top surface of diamond particles. As such, the faceting in the interfacial region was governed by the growth of diamond. The SAD patterns obtained from diamond and nickel substrate, both taken with the primary beam parallel to [011] direction, are also shown in Fig. 7. The two patterns were obtained by translating the sample under the beam without the change of the tilt angle. Although the intensity of the SAD pattern obtained from nickel substrate is not perfectly centered, the pattern still belongs to the same zone axis as that obtained from diamond and, as such, confirms the epitaxial relationship between diamond and nickel lattice. The top to bottom variation in the spot intensity may have arisen due to a rapid increase of the thickness of the sample at the edge of the thinned region. The transparent Ni region is relatively narrow and, as such, the diffraction aperture partially covered also the less transparent part of the sample.

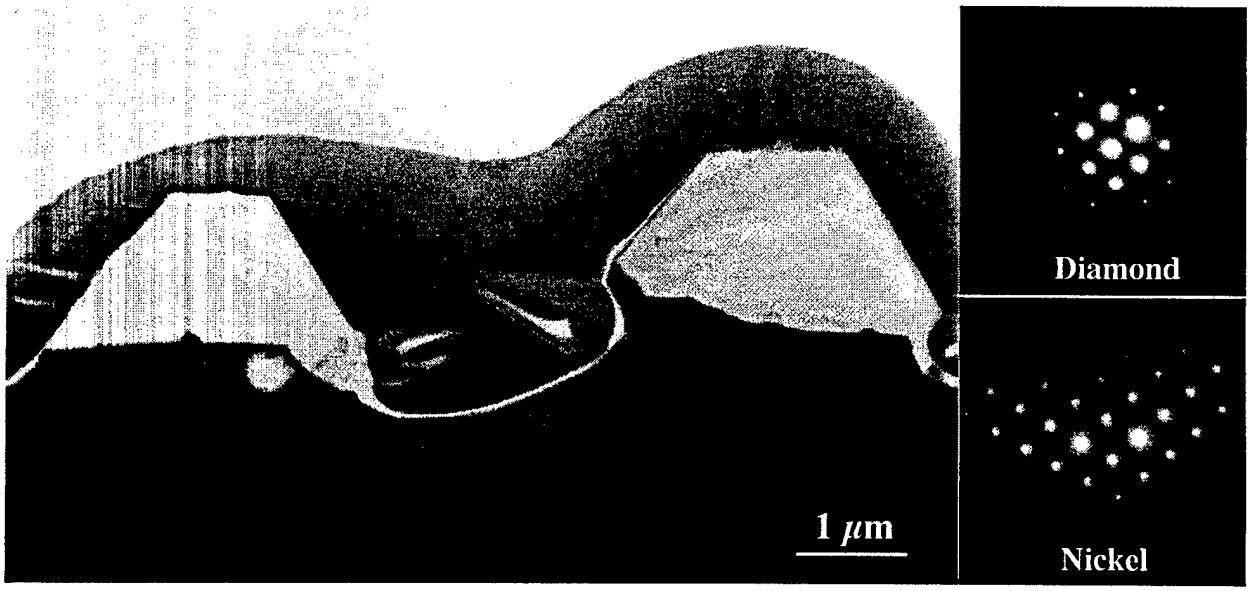


Figure 7. Cross-section TEM of epitaxial diamond particles on nickel with SAD patterns originating from diamond and nickel substrate.

D. Conclusions

Epitaxially oriented diamond has been grown on (100) nickel substrates by a multistep process. The most important part of the process was high temperature annealing. During this step, a low temperature Ni-C-H surface eutectic formed which aided in rapid dissolution of the seeds. Monitoring of the process by optical signals allowed precise timing which was crucial for the achievement of high density of oriented nuclei. The supersaturation of carbon was confined to a thin (<1 μm) surface region as confirmed by Auger spectroscopy and TEM. When cooled, supersaturated carbon segregated and formed coherent $Ni_4C$ precipitates. These precipitates are believed to be the precursor for the nucleation of oriented diamond on nickel. After the prolonged growth, perfectly epitaxial diamond on nickel was obtained, as confirmed by cross sectional TEM analysis.

Although a perfect epitaxial relationship between the diamond and nickel lattice was confirmed, more work is needed to determine the role of $Ni_4C$ on the epitaxial relationship.

E. References


1. P. C. Yang, W. Zhu and J. T. Glass, J. Mater. Res. **8**, 1773 (1993).
2. P. C. Yang, W. Liu, R. Schlesser, C. A. Wolden, R. F. Davis, J. T. Prater, and Z. Sitar, Appl. Phys. Lett. **70**, (1997).
3. P. C. Yang, W. Zhu and J. T. Glass, J. Mater. Res. **9**, 1063 (1994).
4. R. H. Wentorf, Jr., Adv. Chem. Phys. **9**, 365 (1965).
5. H. Li. D. Pugh, J. Lees and J. A. Bland, Nature **4791**, 865 (1961).
6. D. N. Belton and S. J. Schmieg, J. Appl. Phys. **66**, 4233 (1989).
7. Y. Sato, H. Fujita, T. Ando, T. Tanaka and M. Kamo, Philosophical Transactions of the Royal Society of London A **343**, 225 (1993).
8. T. Tachibana, Y. Yokota, K. Nishimura, K. Miyata, K. Kobashi, and Y. Shintani, Diamond and Rel. Mater. **5**, 197 (1996).
9. P. J. Goodhew, *Thin Foil Preparation for Electron Microscopy*, Elsevier, New York, 1985.
10. W. A. Weimer, F. M. Cerio, and C. E. Johnson, J. Mater. Res. **6**, 2134 (1991).
11. H. Lafitau, P. Gendrel, and L. Jacque, Acad. Sc. Paris, Ser. C **263**, 1033 (1966).
12. M. Singleton and P. Nash, Bulletin of Alloy Phase Diagrams **10**, 121 (1989).

# III. Characterization of Copper–Diamond (100), (111) and (110) Interfaces: Electron Affinity and Schottky Barrier

P. K. Baumann and R. J. Nemanich
Department of Physics
North Carolina State University
Raleigh, North Carolina 27695-8202 USA

Abstract

In this study, ultraviolet photoemission spectroscopy (UPS) was employed to correlate the electron affinity and Schottky barrier height of Cu films on type IIb (p-type) diamond (100), (111) and (110) surfaces. Furthermore, field emission measurements were correlated with the effective electron affinity of the samples. Prior to deposition the diamond samples were cleaned by various anneals and plasma treatments in ultra high vacuum (UHV). Annealing the diamond substrates to 1150°C resulted in adsorbate free surfaces with a positive electron affinity. A negative electron affinity (NEA) was induced after depositing 1Å of Cu on the clean surface. The Schottky barrier heights for the clean surfaces ranged from 0.30 eV for the (111) surface to 0.70 eV for the (100) surface. Depositing Cu onto H terminated surfaces exhibiting a NEA still resulted in an NEA on all surfaces. However the Schottky barrier heights were larger, ranging from 0.50 eV for the (111) to 0.90 eV for the (100) and (110) surfaces. The metal induced NEA has been found to be stable to exposure to air. Following a 500°C anneal, an oxygen terminated (100) surface with a positive electron affinity was obtained. Cu deposition resulted in a positive electron affinity and the largest Schottky barrier height with 1.60 eV. A field emission threshold field of 79 V/μm was obtained for an oxygen terminated diamond (100) surface. Values of 20 V/μm, 25 V/μm and 53 V/μm were measured for Cu on clean, H - and O terminated surfaces, respectively. Based on these experiments, it is suggested that chemisorbed species like H or O on diamond surfaces cause an increase in the Schottky barrier, as well as in the field emission threshold field after Cu deposition.

## A. Introduction

The properties of metal-diamond interfaces are of interest for possible applications in electronic devices based on diamond. Previous studies have reported ohmic and rectifying characteristics on oriented, as well as polycrystalline diamond surfaces [1-9]. Diamond has also been considered for cold cathode electron emission applications. Recent results have demonstrated that thin metal overlayers can be employed to achieve a negative electron affinity (NEA).

Copper is of interest since it exhibits a FCC crystal structure with a close lattice match with diamond (a(dia)=3.567Å, a(Cu)=3.615Å). Epitaxial deposition of Cu on diamond (100)

*Submitted to Phys. Rev. B*

surfaces has been reported [10]. There have also been studies of attempting to grow heteroepitaxial diamond on copper. In addition, the relatively low workfunction of Cu (4.48eV) could enable the formation of a NEA on diamond surfaces prepared with different surface terminations.

To understand both rectifying and ohmic contacts it is necessary to determine the Schottky barrier height of the metal semiconductor interface. Because current-voltage characteristics of metal-semiconductor junctions often exhibit high ideality factors, these measurements are often not suitable to obtain the Schottky barrier height. Recently, photoemission spectroscopy has been employed successfully to determine the Schottky barrier height of metal-diamond interfaces.

It has been found that in some instances, diamond exhibits a negative electron affinity. This situation implies that electrons in the conduction band can be emitted directly into vacuum without overcoming an energy barrier. In essence, the electron affinity of a semiconductor represents the band offset between free electrons in the vacuum and the conduction band of the semiconductor, and a NEA represents the situation when the vacuum level is situated below the conduction band minimum. Photoemission has been found to be a very sensitive technique to distinguish between a NEA or positive electron affinity.

Prior studies have shown that deposition of a few Å of a metal like Ti, Ni, Co, Cu or Zr on diamond can induce a negative electron affinity (NEA) [11-18]. In particular, it has been found that thin layers of Ti or Ni on clean (111) surfaces resulted in a NEA. Reports of preliminary studies of films of Cu, Co and Zr on diamond have also indicated the possibility of an NEA, and these results suggested that the initial diamond surface preparation played a role in the effect. Furthermore, lower Schottky barrier heights have been reported for metal films deposited on adsorbate free surfaces than for surfaces terminated by species such as hydrogen or oxygen.

Interfaces between metals and semiconductors can be described in general by different models. An ideal metal-semiconductor interface is often described by the Schottky-Mott model, also called the workfunction model. In this model,the Schottky barrier height is determined by the metal workfunction and the semiconductor electron affinity. It is assumed that the atomic structure of the interface is the same as for the free surface, and that the interface bonding does not cause any defects. It also is assumed that there are no surface states on the semiconductor surface. Thus, the difference between the metal workfunction and the semiconductor electron affinity does not change when the interface is formed. Then for a p-type semiconductor, the Schottky barrier height $\Phi_B$ is described by

$$\Phi_B = E_G - (\Phi_M - \chi), \qquad (1)$$

where $E_G$ is the band gap and $\chi$ the electron affinity of the semiconductor, and $\Phi_M$ is the metal workfunction.

Other models are based on interface dipoles. One possibility is that the metal and semiconductor are separated by an insulating layer and that there are surface states on the semiconductor surface. For a large surface density of states, the Fermi level is pinned by the surface states, and the Schottky barrier height is independent of the workfunction of the metal. For this case, different metals will exhibit very similar or even identical values for the Schottky barrier height.

Consider a thin layer of metal on a semiconductor such that electrons leaving the semiconductor can tunnel through the metal film. Then, the metal can be thought of as causing a surface dipole which affects the effective electron affinity of the semiconductor with respect to the vacuum. This situation may be represented by two interfaces—the vacuum-metal interface and the metal-semiconductor interface. If the metal-semiconductor interface is such that the vacuum level lies below the conduction band minimum, then this interface structure exhibits a NEA. Whether such a structure exhibits a positive electron affinity or a NEA may depend on the semiconductor surface (such as surface adsorbates, surface states and surface structure) prior to metal deposition and on the metal itself.

A theoretical study of Cu on clean and H-terminated diamond (111) surfaces has been presented by Lambrecht [19]. A value of the Schottky barrier height of less than 0.1 eV was predicted for the most stable configuration for the clean surface. Whereas a Schottky barrier of greater than 1.0 eV was calculated for Cu on a hydrogenated surface.

The formation of a cold cathode structure will typically require a field emission structure. In the experiments described here, field electron emission measurements are obtained by bringing a metal anode in close proximity to the sample and applying a bias between the two. Then the emission current vs. applied voltage is recorded. The mechanism for field emission is more complicated than for photoemission spectroscopy. Here the injection of electrons into the semiconductor, the transport of these electrons through the bulk to the emitting surface and the actual emission from the surface into vacuum need to be considered. Consider the case of a NEA surface. If the field emitted electrons are emitted from the conduction band minimum then the electrons do not encounter a barrier when leaving the surface. The field electron emission would be limited only by the injection and transport processes.

For the diamond (111) 1×1:H surface, simultaneous photoemission and field emission measurements have been reported. This surface exhibits a NEA, but it was found that the field emitted electrons originated from the valence band. Assuming this is the case, then the electrons still may have to overcome (or tunnel through) a surface barrier when being emitted into vacuum even for a NEA surface. A NEA would only contribute to lowering this surface barrier, but may not entirely remove it.

We report here a comprehensive study of thin Cu films deposited on diamond (100), (111) and (110) surfaces. Before deposition, the diamond surfaces have been cleaned by various anneals and plasma cleans. These treatments result in surfaces terminated with oxygen, hydrogen or free of surface adsorbates. The surface properties were analyzed before and after Cu deposition. The UV photoemission results are employed to understand the relationship of the Schottky barrier height and the presence of a NEA. In addition, the results from UV photoemission and field electron emission are compared.

B. Experimental Details

Natural type IIb single crystal semiconducting, boron doped diamond (100), (111) and (110) substrates were used. Typical resistivities of these samples were $10^4$ Ω cm. The wafers were 3×3×0.25 mm in size and were polished with 0.1 μm diamond grit.

An electrochemical etch has been employed to remove non-diamond carbon and metal contaminants [20]. For this purpose, the diamond samples have been placed in deionized (DI) water as an electrolyte between two Pt electrodes. To facilitate this cleaning step, a DC bias of 350 V was applied between the electrodes. This resulted in a current of about 0.5 mA. Subsequently, the crystals were dipped in HF solution to remove oxides from the surface [21]. Silicon dioxide contaminants have previously been detected following an electrochemical etch [21]. Small amounts of these contaminants may be present in the DI water and may originate from the ion exchanger matrix used to prepare the DI water. After the wet chemical etch, the substrates were blown dry with $N_2$, mounted on a Mo holder and transferred into the UHV system. This UHV system consists of several chambers connected by a UHV transfer system. These capabilities include annealing, H plasma treatment, metal deposition, angle-resolved ultraviolet photoemission spectroscopy (ARUPS), Auger electron spectroscopy (AES) and low energy electron diffraction (LEED).

To study the effect of surface preparation on the characteristics of copper-diamond interfaces, three different *in situ* cleaning processes were used. Each of these treatments was employed on the diamond substrates before copper deposition. One procedure included an anneal to 500°C for 10 min. Another involved annealing the substrates to 1150°C for 10 min. The base pressure in the annealing chamber was $1\times10^{-10}$ Torr and rose to $8\times10^{-10}$ Torr and $7\times10^{-9}$ Torr during the 500 and 1150°C anneals, respectively. The temperature was measured using an optical pyrometer focused on the Mo plate holding the sample. The third surface cleaning process consisted of a H plasma exposure. During this process, the sample was held at 500°C. The H plasma was remotely excited by a rf induction coil. Remote excitation results in significantly lower ion and electron densities at the surface of the samples. The details of the plasma system have been discussed previously [22]. The surface morphology was

characterized with AFM. Linear groves of ~ 20 Å in depth were detected on the diamond substrates. These are attributed to the polishing process with diamond grit.

The photoemission spectra were excited with HeI (21.21 eV) radiation. A 50 mm VSW HAC50 hemispherical analyzer with an energy resolution of 0.15 eV and an acceptance angle of 2° was employed to measure the emitted electrons. A bias of up to 1 V was applied to the sample to overcome the workfunction of the analyzer. This enabled the detection of the low energy electrons emitted from the NEA surfaces. These electrons appear as a sharp peak at the low energy end of UPS spectra. The position of this feature corresponds to the energy position of the conduction band minimum, $E_C$ (Fig. 1). Emission from $E_C$ is positioned at $E_V + E_G$ in the spectrum, where $E_V$ is the energy of the valence band maximum and $E_G$ that of the bandgap. Furthermore, electrons from $E_V$ are photoexcited to an energy level at $E_V + h\nu$ in the conduction band and are detected at $E_V + h\nu$ in the UPS spectra. This corresponds to the high kinetic energy end of the spectra. The spectral width for a NEA surface or the distance between emission from the valence band maximum and the conduction band minimum is therefore $h\nu - E_G$. Using the values for He I radiation $h\nu = 21.21$ eV and the bandgap of diamond $E_G = 5.47$ eV, a spectral width of ~ 15.7 eV is predictive of a NEA. For the case of a positive electron affinity surface, the vacuum level determines the low energy cutoff. This results in a smaller spectral width [1, 23].

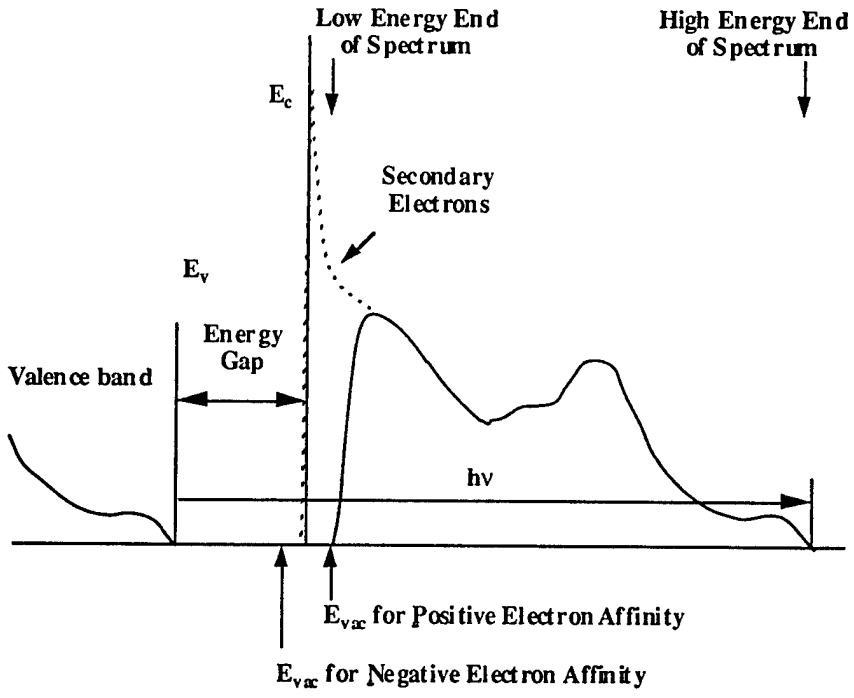


Figure 1. Schematic diagram of photoemission spectra for a negative electron affinity surface (dotted line) and a positive electron affinity surface (solid line).

Photovoltaic effects may cause shifts in the UPS spectra, especially for wide bandgap semiconductors like diamond or for low temperature measurements [24]. These effects have been demonstrated recently for the diamond (111) surface [25]. These shifts are, however, uniform for the entire spectrum, and the relative distance between the valence band maximum and the low energy cutoff will not change.

For p-type semiconductors like diamond, the Schottky barrier height $\Phi_B$ is determined by the difference between the position of the valence band maximum $E_V$ of the semiconductor and the Fermi level of the metal (Fig. 2). The Schottky barrier height $\Phi_B$ can, therefore, be deduced from a photoemission spectrum that exhibits features from both the semiconductor and the metal. Thus, no corrections for photovoltaic effects need to be made. To determine the Schottky barrier height in this way, the thickness of the metal layer has to be equal to or less than the electron mean free path ( $\leq 5$ Å). But even for metal thicknesses of less than the mean free path, the metal Fermi level may obscure the relatively weak onset of emission at $E_V$. Independently, $E_V$ can be referenced to strong peaks in the diamond spectrum that can clearly be detected even after metal deposition. We have chosen a feature positioned at 8.3 eV below $E_V$. For this correlation to be valid the relative distance between the bulk feature and $E_V$ must not change in spectra taken before and after metal deposition. In addition, for a NEA the position of the low energy peak (which corresponds to $E_C$) can be used as a reference to locate $E_V$ (which is the high energy end of the diamond spectrum). And the distance between $E_C$ and $E_V$ in the spectrum has to be $h\nu - E_G$ (Fig. 2). A change in band bending (e.g. due to metal

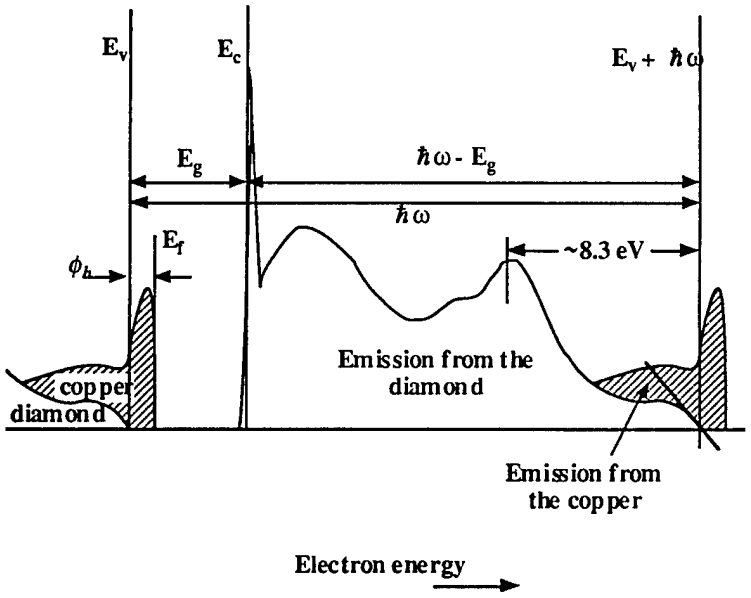


Figure 2. Schematic diagram of photoemission spectra for copper deposited on diamond. The Schottky barrier height $\Phi_B$ is determined from the difference between the position of the valence band edge of diamond $E_V$ and the metal Fermi level $E_F$.

deposition) can be detected as a shift of the spectrum with respect to the Fermi level. Again since the position of $E_V$ may be difficult to discern such a shift can be detected from the position of bulk features in the spectra.

Field emission measurements were carried out in a separate vacuum chamber with a base pressure of ~ $2\times10^{-8}$ Torr. The I-V characteristics were determined by applying a bias of 0–1100V between the sample and a 2 mm diameter stainless steel anode with a rounded tip. A Keithley 237 source-measuring unit was employed for the I-V measurements. The distance between the sample and the anode could be varied in vacuum by a stepper motor. Typical distances were 2 - 30 μm.

Cu films of 1, 2, 3, 6, 10 Å thickness have been deposited by e-beam evaporation. AES was employed to confirm the presence of a Cu layer. Following each deposition step, the samples were characterized by means of UPS. In the metal deposition chamber, the pressure was $1\times10^{-10}$ Torr, and the pressure rose to $8\times10^{-9}$ Torr during deposition. The growth rate was determined by a quartz crystal monitor. Typical values were ~ 0.1 Å/s for thicknesses up to 3 Å and ~ 0.2 Å/s for thicknesses of 6 and 10 Å. Most of the samples were held at room temperature during deposition. To check if the morphology or epitaxy of the Cu films depended on the substrate temperature during deposition, some samples were heated to 500°C during Cu overgrowth. We also studied the effects of air exposure on the samples. For this purpose the UPS measurements were repeated on samples that were taken out of the UHV system. It was of particular technological interest to determine whether NEA characteristics of some samples would be stable in air.

C. Results

*Diamond Surfaces.* The photoemission of the diamond terminated surfaces has been reported elsewhere but is briefly summarized here [1, 23, 26-30]. Consider first the termination of the surfaces before Cu deposition. Annealing the C(100) samples to 500°C does not significantly reduce the oxygen peak in the AES spectra, and the LEED measurements indicated a 1×1 unreconstructed or bulk pattern. After annealing to 1150°C, the oxygen feature could no longer be detected, a 2×1 LEED pattern is observed, and the surface is presumed clean of adsorbates. A H terminated 2×1 surface could be induced by H-plasma exposure either after the 500°C or after the high temperature anneal. The electron affinity was deduced from the UPS measurements. An electron affinity of $\chi \cong 0.7$ eV was found for the adsorbate free and of $\chi \cong 1.45$ eV for the oxygen terminated surfaces. A NEA was detected subsequent to the H plasma exposure. In addition, an emission feature at ~ 0.4 eV below the conduction band minimum ($E_C$) was observed in the spectrum of the H terminated surface. It was suggested that this feature could be due to emission sites near the conduction band or due to spatial variations in the surface Fermi level.

For the diamond (111) samples, annealing to 1050°C results in an adsorbate free surface with a 2×1 LEED pattern. A positive electron affinity of $\chi \cong 0.5$ eV was measured from UPS spectra. A H plasma clean results in a NEA. These results are consistent with previous studies on surface cleaning and UV photoemission measurements of diamond (111) samples [1, 2, 4]. Following the H plasma exposure, we also measured emission ~ 0.4 eV below $E_C$.

For the diamond (110) surfaces, an adsorbate free surface was observed after an 1150°C anneal. The UPS indicated a positive electron affinity of $\chi \cong 0.7$ eV. After a H plasma exposure the UPS indicated an NEA, and again the low energy end of the spectrum extended to ~ 0.4 eV below $E_C$.

*Copper on Diamond.* Subsequent to depositing 1Å of Cu onto the clean (100) surface the width of the photoemission spectrum increased consistently with a NEA (Fig. 3). A bulk feature of the diamond (labeled B) was used as a point of reference to determine shift of the spectra. After the initial 1Å deposition, the spectrum was observed to shift by 0.3 eV to lower energies with respect to the Fermi level. The energy difference between feature B and the valence band maximum was observed to be unchanged. This difference is expected to remain constant for thicker copper layers. The spectral shift is indicative of a change in Fermi level pinning at the surface. As the Cu thickness is increased, the emission from the copper d-bands is observed, and the Fermi level is easily detectable. A Schottky barrier height of $\Phi_B \cong 0.70$ eV was determined from the UPS spectra. This value remained constant for the different thicknesses of the Cu films. Thus, the pinning position of the Fermi level did not change with the thickness of the Cu layer. The thicker layers of Cu up to 10 Å still resulted in a NEA, however, the intensity of the low energy emission was reduced. In addition, the bulk features of diamond became less pronounced with increased Cu coverage.

For the H terminated (100) surface the NEA peak was still observed after Cu deposition for all Cu thicknesses (Fig. 4). However, the peak intensity continued to decrease with increasing Cu coverage. In addition, the emission below $E_C$ was reduced with increasing thickness of the Cu film until it was no longer detected for a thickness of 10 Å of Cu. In fact, the low energy cutoff was reduced by ~ 0.4 eV in the spectra for 10 Å of Cu as compared to 1Å of Cu. The Schottky barrier height was found to be $\Phi_B \cong 0.90$ eV, and the shift in the spectra following metal deposition was 0.6 eV towards lower energies.

In comparison to Cu on the clean and H terminated C(100) surfaces, 1Å of Cu on the oxygen terminated (100) surfaces resulted in a positive electron affinity (Fig. 5). The electron affinity was, however, reduced from $\chi \cong 1.45$ eV for the oxygen terminated surface to $\chi \cong 0.75$ eV after Cu deposition. The spectrum was observed to shift by ~ 0.6 eV to lower energies. A value of 1.60 eV was determined for the Schottky barrier height. The intensity of the bulk diamond features decreased for increasing thickness of the Cu layers. LEED patterns could still be observed following deposition.

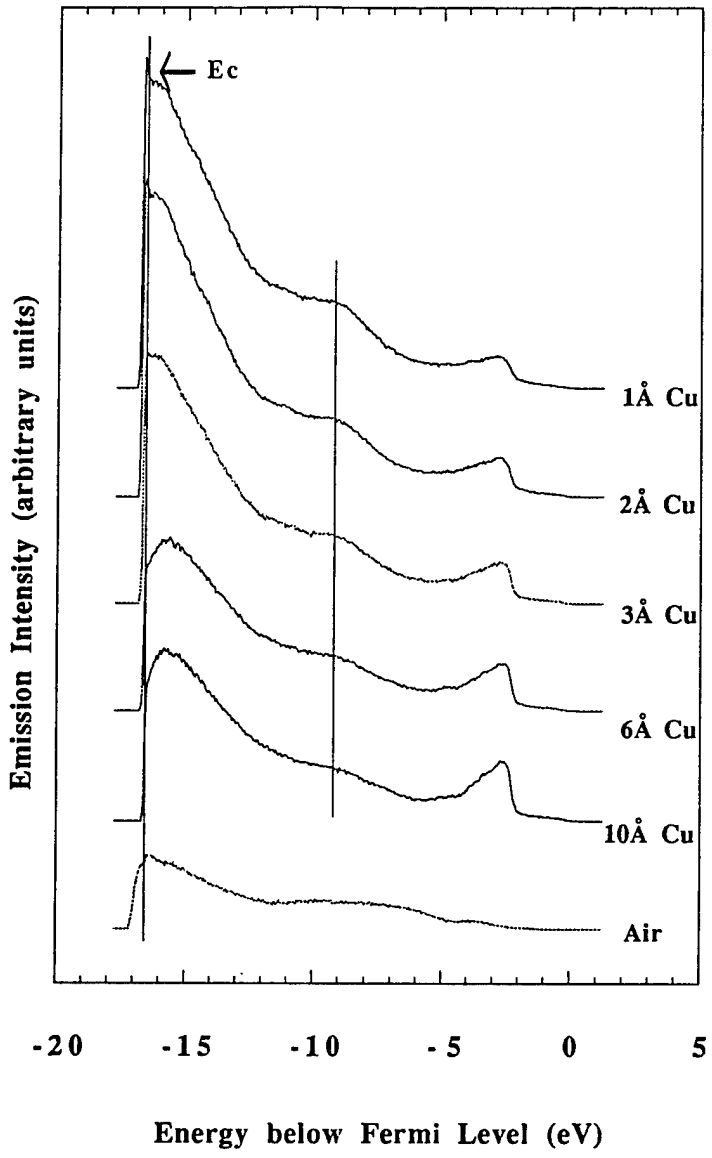


Figure 3. UV photoemission spectra of copper on a clean diamond (100) surface. The diamond surface exhibits a positive electron affinity before Cu deposition. Subsequent to Cu deposition, the width of the spectrum increases and a NEA is detected. After air exposure, the NEA is still observed.

Depositing Cu on the clean (111) surface did not result in a shift of the UPS spectra. The low energy edge of the spectrum extended to lower energies, consistent with a NEA. The NEA was still observed for 10 Å thick Cu films, however, with decreased intensity. A Schottky barrier of $\Phi_B \cong 0.30$ eV was measured which did not change for increasing thickness of the Cu films.

After depositing Cu onto the H covered (111) surface, the UPS spectra still indicated the presence of a NEA, even for 10 Å thick layers (Fig. 6). However, the emission below $E_c$

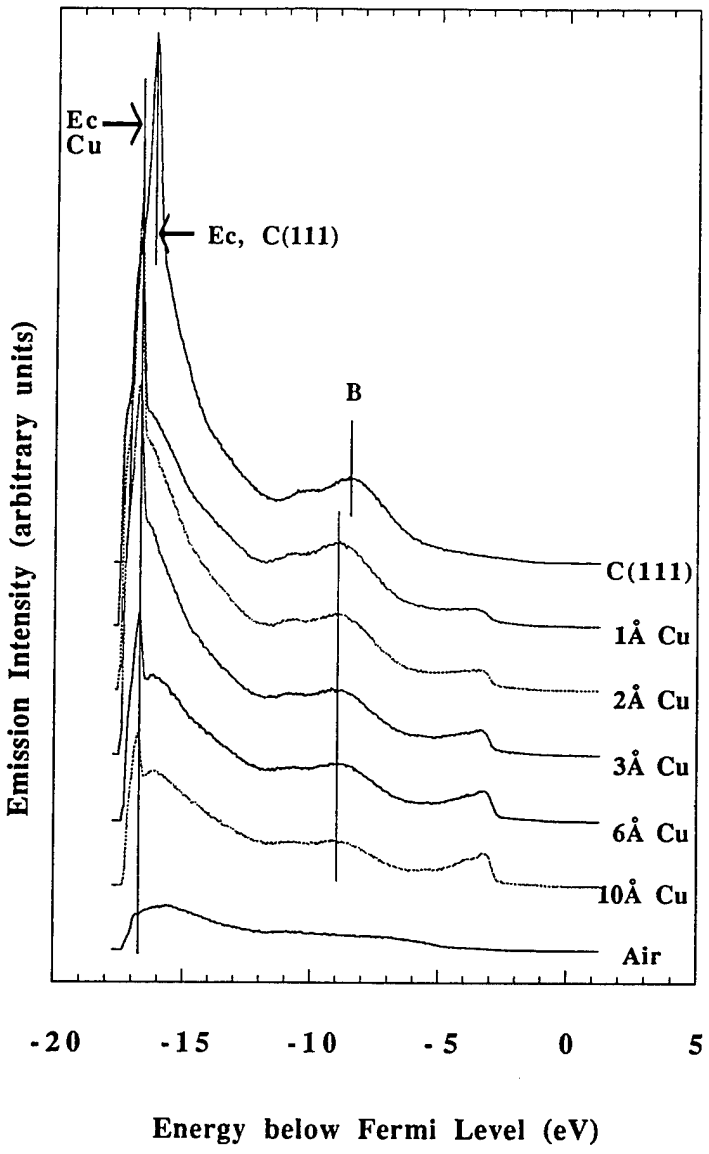


Figure 4. UV photoemission spectra of copper on a hydrogen terminated diamond (100) surface. The diamond surface exhibits a NEA before Cu deposition. Also, emission below $E_c$ is detected. Following Cu deposition, the NEA is still observed, however, the emission below $E_c$ gets reduced with increasing thickness of Cu. After air exposure, the NEA is still detected.

decreased significantly with increasing Cu coverage and was no longer observable for 10 Å of Cu. The spectra shifted 0.2 eV to lower energies upon Cu deposition, and a Schottky barrier of $\Phi_B \cong 0.50$ eV was determined. The Cu–on–diamond films exhibited LEED patterns.

Similar to the (100) and (111) samples, the deposition of Cu on the clean (110) surface resulted in the indication of a NEA that was still observable for 10 Å thick films (Fig. 7). A shift of ~ 0.2 eV to lower energies due to Cu was determined, and the Schottky barrier was measured to be $\Phi_B \cong 0.60$ eV.

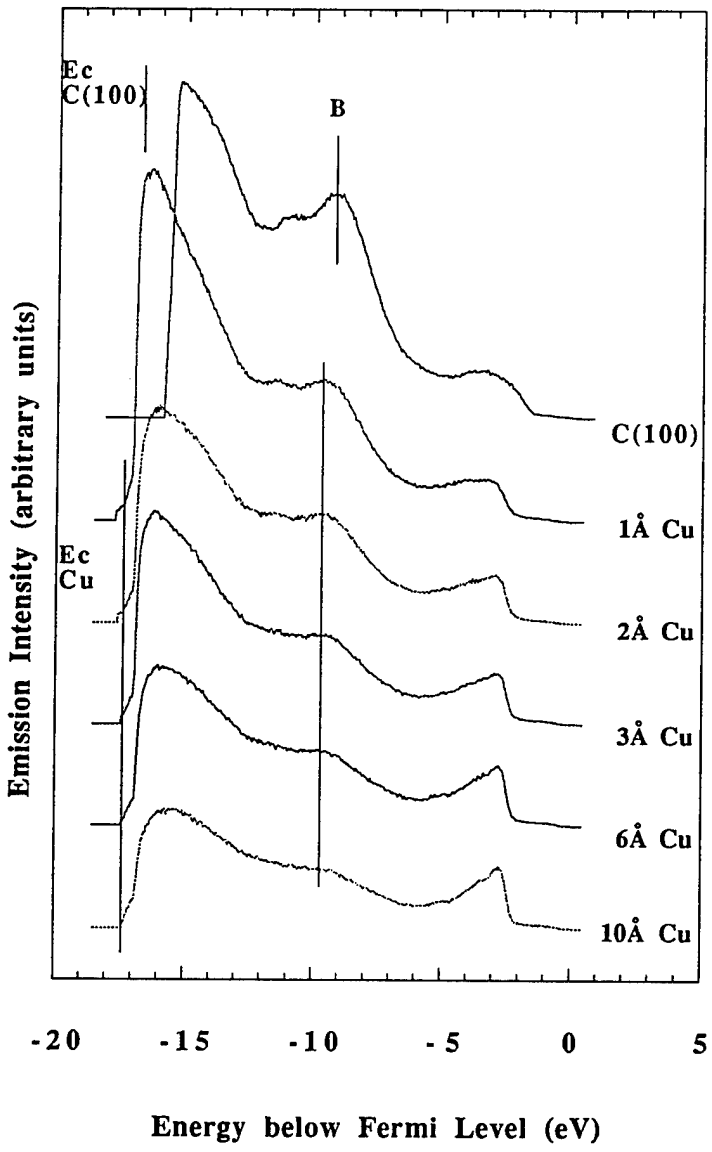


Figure 5. UV photoemission spectra of copper on an oxygen terminated diamond (100) surface. The diamond surface exhibits a positive electron affinity prior to Cu deposition. Subsequent to Cu deposition, the width of the spectrum increases somewhat, but the spectra still exhibit a positive electron affinity.

Corresponding to the (100) and (111) surfaces the NEA peak could still be detected after deposition of Cu onto the H terminated (110) surface, even for layers of 10 Å in thickness. A shift in the spectra of 0.6 eV was observed following Cu deposition. Also, the low energy cutoff shifted, reducing the width of the spectrum by ~ 0.4 eV for the thick Cu layers. Subsequent to Cu deposition LEED patterns were still detected.

Consider the case of Cu deposition on clean diamond (100) substrates at 500°C (Fig. 8). Deposition of 1Å of Cu resulted in a shift of the spectra by 0.1 eV to lower energies. While the width of the spectrum increased, only weak emission was detected at the energy position of the

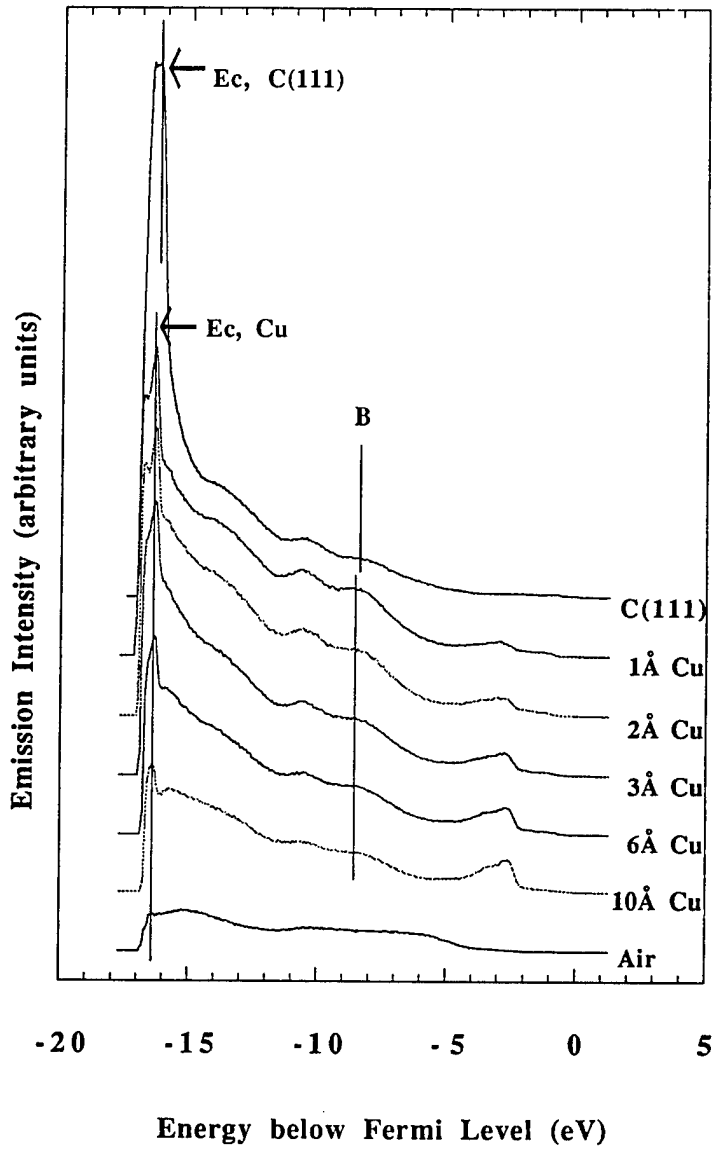


Figure 6. UV photoemission spectra of copper on a hydrogen terminated diamond (111) surface. The diamond surface exhibits a NEA before Cu deposition. Also, emission below $E_c$ is detected. Following Cu deposition, the NEA is still observed, however, the emission below $E_c$ gets reduced with increasing thickness of Cu. After air exposure, the NEA is still detected.

conduction band minimum. Subsequent to depositing more Cu, an additional increase in the width of the spectrum consistent with a NEA was observed. For 10Å thick layers of Cu, the spectra still indicated a NEA. The spectra shifted by an additional 0.2 eV, and the measured Schottky barrier height of $\Phi_B \equiv 0.75$ eV corresponds to the value obtained for Cu deposition on the clean diamond (100) surface at room temperature. LEED patterns were detected from the Cu-on-diamond films. All UPS results are summarized in Table I.

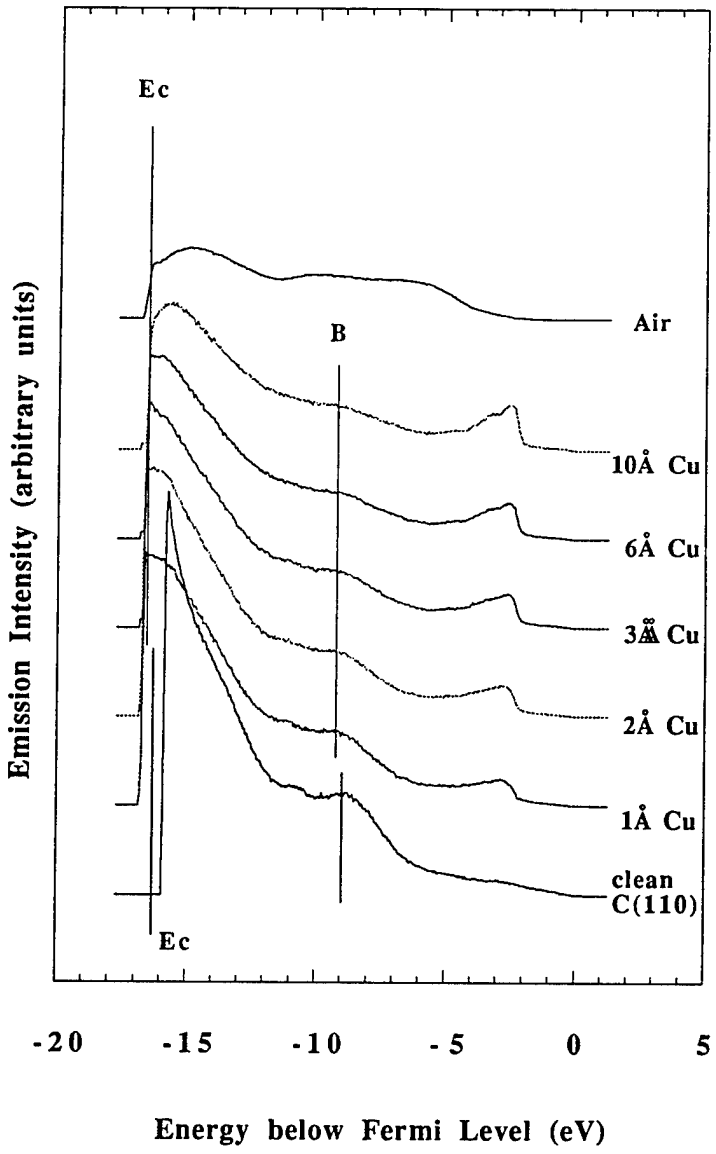


Figure 7. UV photoemission spectra of copper on a clean diamond (111) surface. The diamond surface exhibits a positive electron affinity before Cu deposition. Subsequent to Cu deposition, the width of the spectrum increases and a NEA is detected. After air exposure, the NEA is still observed.

We have previously reported that 300 and 2000Å of Cu deposited on diamond (100) substrates at 500°C exhibited 1×1 LEED patterns. By using AFM, islands oriented with respect of the substrate were detected [10]. In particular, well defined islands of ~ 10000 Å x 5000 Å in size were observed for the 2000Å thick Cu layers. By means of Rutherford backscattering, we have confirmed that these Cu films were epitaxial [10].

AFM scans of the diamond surfaces before Cu deposition exhibited linear groves parallel to each other. These features are attributed to the polishing process with diamond grit. Consider

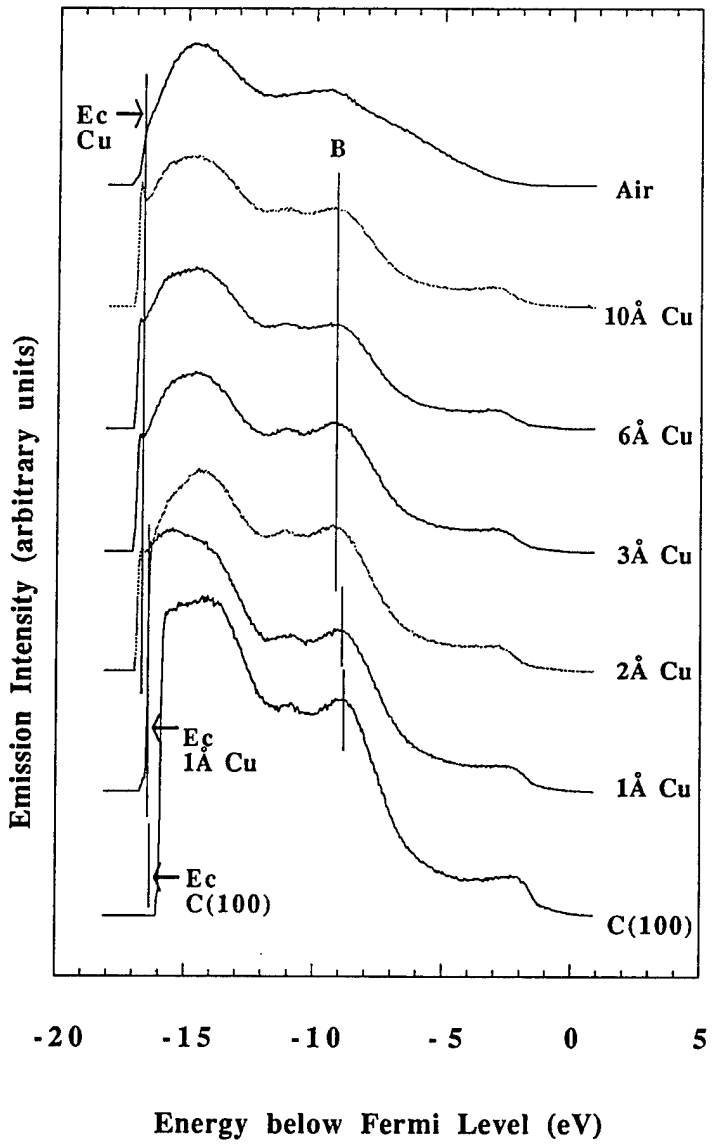


Figure 8. UV photoemission spectra of copper on a clean diamond (100) surface. The substrate was kept at 500°C during Cu deposition. The diamond surface exhibits a positive electron affinity before Cu deposition. Subsequent to Cu deposition, the width of the spectrum increases and a NEA is detected. After air exposure, the NEA is still observed.

first the Cu layers on diamond deposited at room temperature. After depositing 2Å of Cu on diamond no islands could be resolved by AFM (Fig. 9a). Following the overgrowth of 6Å of Cu, islands of ~ 50 Å in diameter were detected on the groves of the diamond substrate (Fig. 9b). For a 40 Å thick Cu layer islands of ~ 100 - 200 Å in size were observed (Fig. 9c) LEED did not show clear diffraction patterns for 40Å of Cu deposited at room temperature. For the case of Cu grown at 500°C islanding could be observed after 2Å had been deposited (Fig. 10a). The islands were ~ 50 to 100 Å in size. An AFM scans after 100 Å of Cu on

Table I. Summary of the UPS measurements. PEA: positive electron affinity, NEA: negative electron affinity. Also the values of the electron affinity $\chi$ calculated according to the workfunction model are listed. The error margins are 0.1 eV.

| Sample surface | UPS before Cu growth | UPS after Cu growth | NEA stable in air | calculated $\chi$ |
|---|---|---|---|---|
| C(100) | | | | |
| clean | PEA, $\chi = 0.7$ eV | NEA, $\chi < 0$, $\Phi_B = 0.70$ eV, 0.3 eV shift | yes | $\chi = -0.20$ eV |
| H terminated | NEA, $\chi < 0$ | NEA, $\chi < 0$, $\Phi_B = 0.90$ eV, 0.6 eV shift | yes | $\chi = 0$ eV |
| O terminated | PEA, $\chi = 1.45$ eV | PEA, $\chi = 0.75$ eV, $\Phi_B = 1.60$ eV, 0.6 eV shift | | $\chi = 0.70$ eV |
| C(111) | | | | |
| clean | PEA, $\chi = 0.5$ eV | NEA, $\chi < 0$, $\Phi_B = 0.30$ eV, no shift | yes | $\chi = -0.20$ eV |
| H terminated | NEA, $\chi < 0$ | NEA, $\chi < 0$, $\Phi_B = 0.50$ eV, 0.2 eV shift | yes | $\chi = 0$ eV |
| C(110) | | | | |
| clean | PEA, $\chi = 0.7$ eV | NEA, $\chi < 0$, $\Phi_B = 0.60$ eV, 0.2 eV shift | yes | $\chi = -0.40$eV |
| H terminated | NEA, $\chi < 0$ | NEA, $\chi < 0$, $\Phi_B = 0.90$ eV, 0.6 eV shift | yes | $\chi = -0.10$ eV |
| C(100) | | deposition at 500°C | | |
| clean | PEA, $\chi = 0.7$ eV | NEA, $\chi < 0$, $\Phi_B = 0.75$ eV, 0.3 eV shift | yes | $\chi = -0.15$ eV |

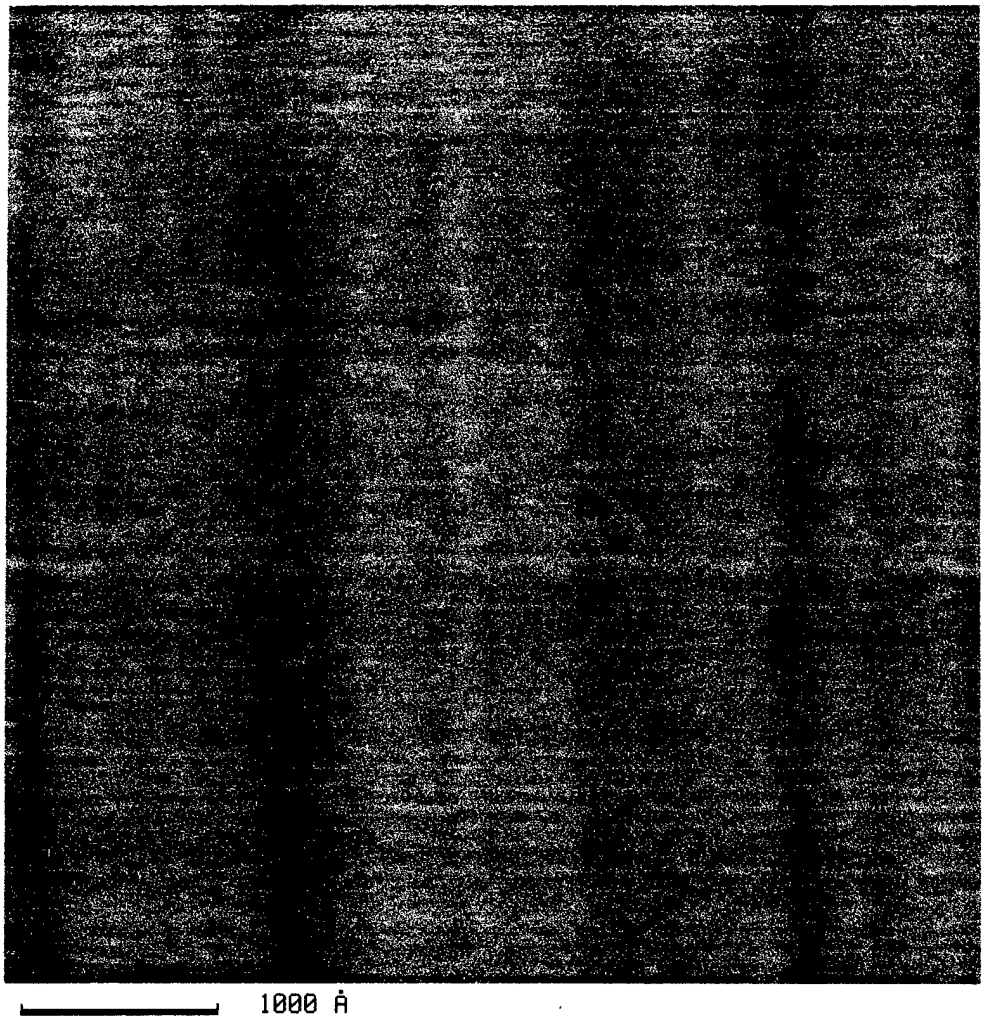


Figure 9a. Atomic force micrograph of 2 Å of Cu on diamond. No island formation is resolved on the polishing grooves of the diamond substrate.

diamond deposited at 500°C displayed oriented islands of ~ 500–1000 Å in size. The islands were oriented along the <110> directions of the underlying diamond (100) substrate (Fig. 10b). The observation of oriented islands is an indication of epitaxial alignment. LEED patterns could be detected for 2Å and 100Å of Cu deposited at 500°C.

The samples of Cu on both clean and H terminated diamond (100), (111) and (110) surfaces were exposed to air and reintroduced for UPS measurements. Even after air exposure, the width of the UPS spectra still corresponded to a NEA. However, the intensity of the low energy emission was reduced. Such a reduction in intensity may be consistent with the presence of physiadsorbed species that are expected to be on the surface from the air exposure. Indeed, AES scans indicated the presence of oxygen following air exposure.

*Field Emission Results.* Field emission measurements were performed on diamond (100) samples and on the 10Å thick Cu films deposited on clean, hydrogen or oxygen terminated diamond (100) surfaces. The I-V data for Cu on the hydrogen terminated diamond surface is

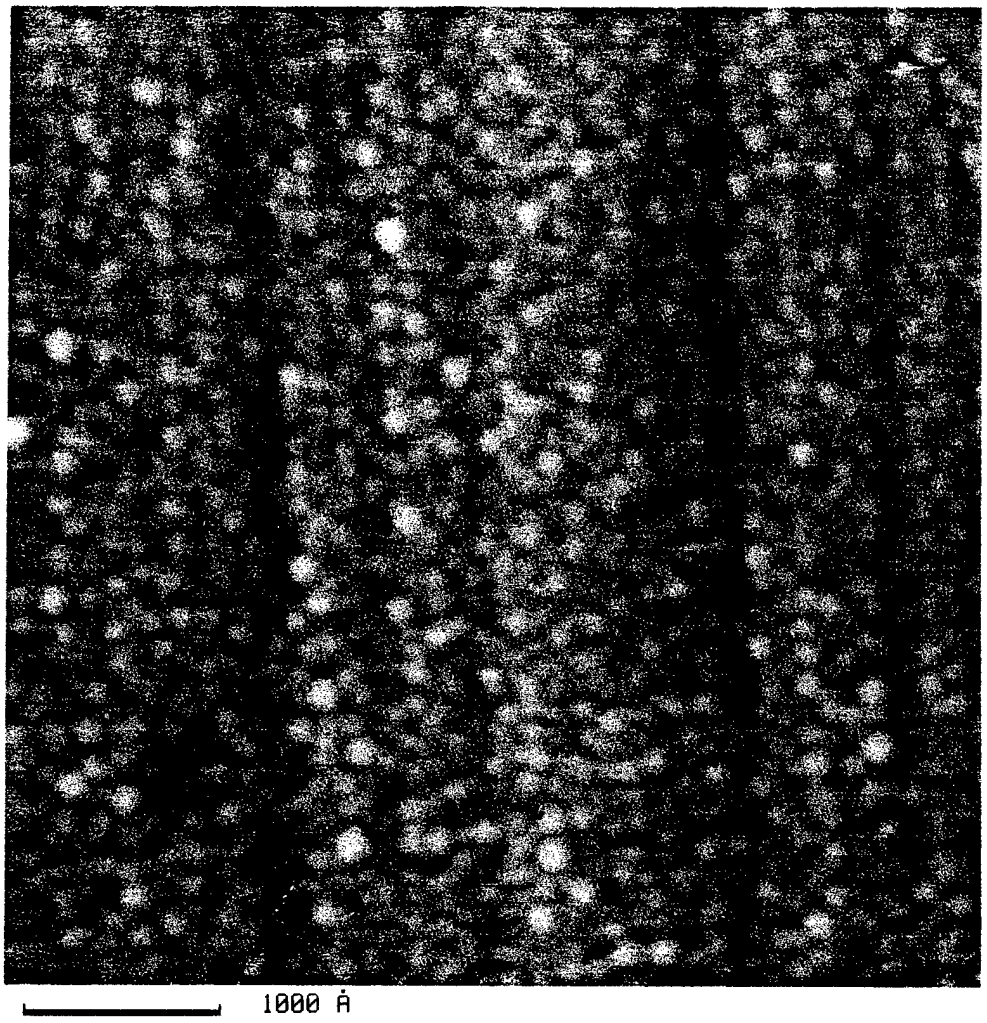


Figure 9b. Atomic force micrograph of 6 Å of Cu on diamond. Islands of ~ 50 Å in diameter are observed.

shown in Fig. 11. For the measurements presented here, the emission threshold voltage has been defined to corresponded to a current of 0.1 μA. This is necessary since the measured current –voltage curves did not exhibit an absolute threshold. Oftentimes the voltage per μm is also called the average field. The average field emission threshold field and corresponding standard deviation were calculated from the values of the emission threshold voltage for different distances. For the distances used here, it was found that the average field was relatively independent of distance.

The results and the standard deviations for the different surface terminations are summarized in Table II. Thresholds between 25 and 79 V/μm were determined. For the oxygen terminated diamond surface the highest value of 79 V/μm was measured. In general, Cu deposition led to a reduction in the threshold field. The lowest threshold of 25 V/μm was obtained for Cu deposited on the clean surface. The next highest value of 35 V/μm was measured for Cu on the hydrogen terminated surface. These two surfaces also exhibited a NEA

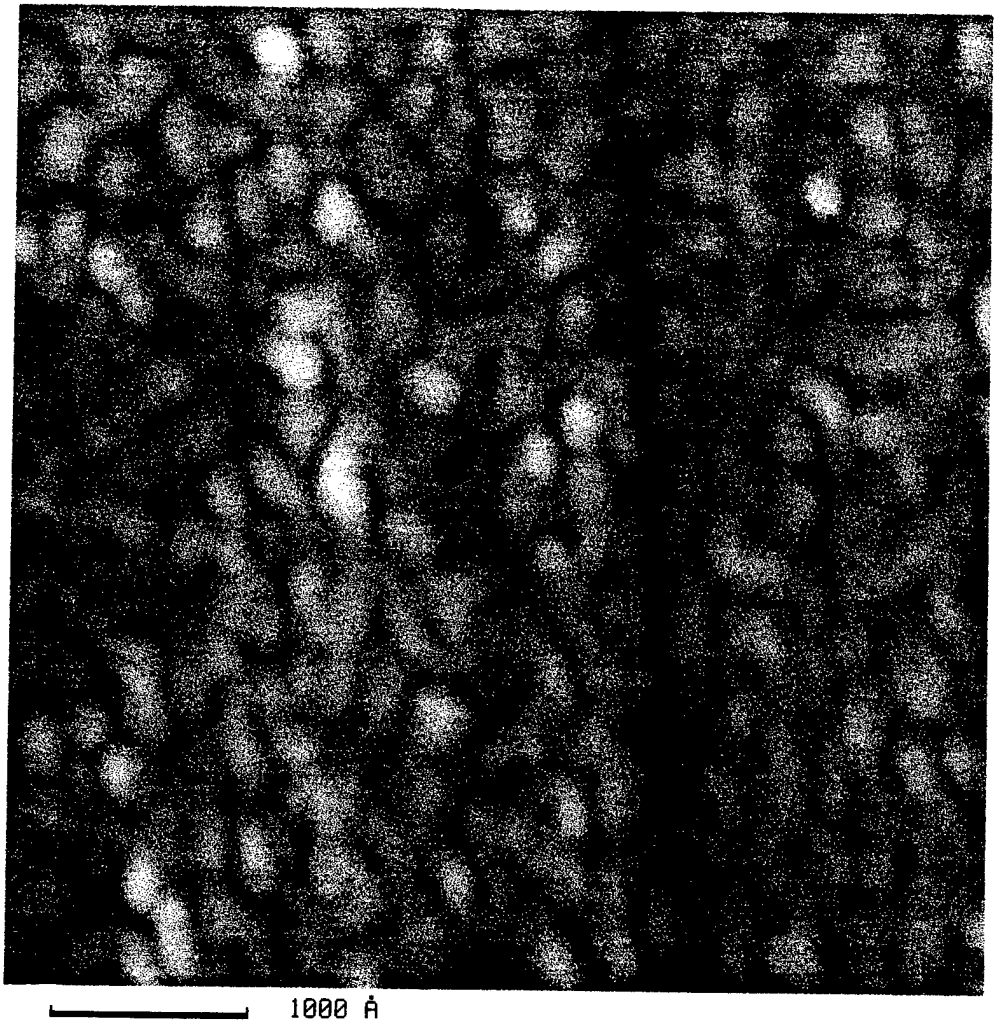


Figure 9c. Atomic force micrograph of 40 Å of Cu on diamond. Islands of ~ 100–200 Å in size are detected.

as determined from UPS spectra. For Cu on the oxygen terminated surface, the measurements indicated the highest value of 53 V/μm for the different Cu-diamond surfaces. Note that the surface exhibited a positive electron affinity.

These results indicate that surfaces exhibiting a NEA also exhibit a lower field emission threshold than those with a positive electron affinity. The threshold value decreased with decreasing electron affinity. Since the actual value of the electron affinity cannot be determined by UPS for a NEA, we may correlate the threshold field with the Schottky barrier height of the Cu–diamond interfaces. From Table II it is evident that threshold does decrease with declining values of the Schottky barrier height.

The values for the field emission threshold reported here are of the same order of magnitude as previously reported for diamond samples [31, 32]. The data from the field emission measurements have been fit to the Fowler-Nordheim equation [33]:

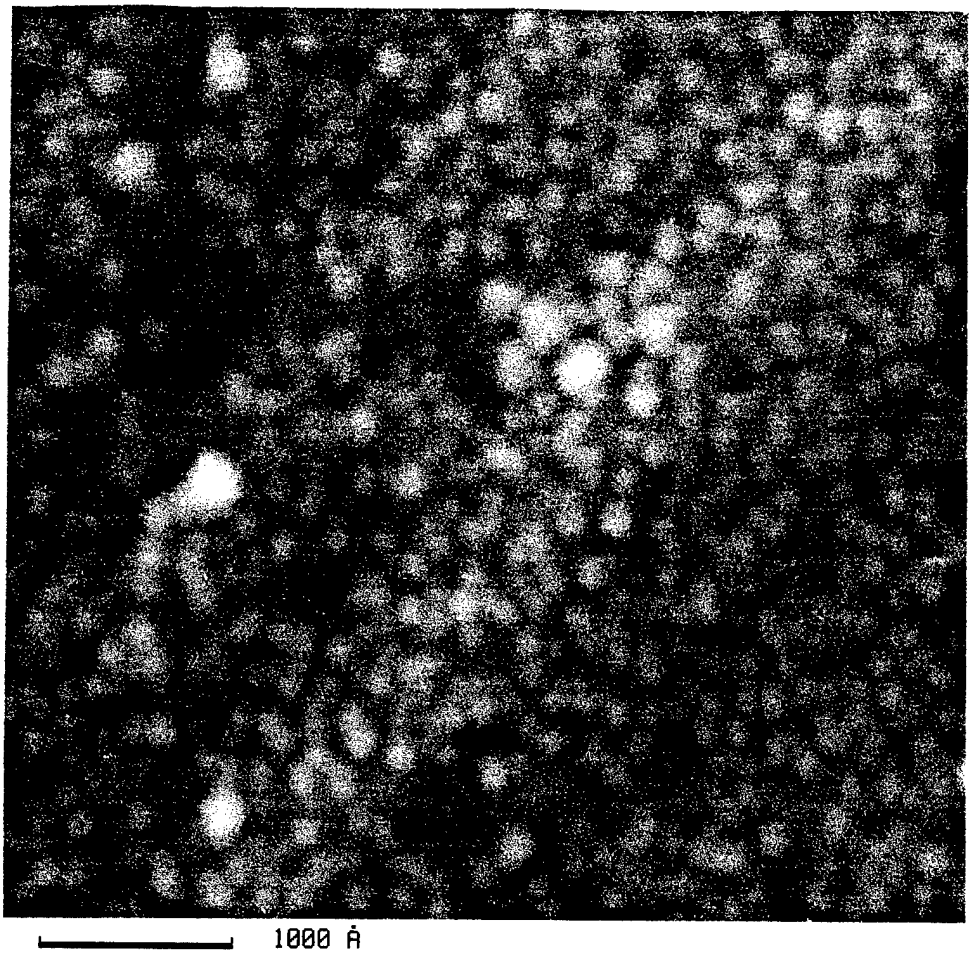


Figure 10a. Atomic force micrograph of 2 Å of Cu on diamond deposited at 500°C. Islands of ~ 50–100 Å in size are detected.

$$I = k\left(\frac{\beta V}{d}\right)^2 \exp\left(\frac{-6.530 d\varphi^{3/2}}{\beta V}\right) \tag{2}$$

where I is the current in amps, V is the bias in volts, d is the distance between the sample and the anode in microns, k is a constant, $\varphi$ is the effective barrier height in eV and $\beta$ is the field enhancement factor. For perfectly flat surfaces $\beta$ is equal to 1 and can be neglected. It should be noted that different surface terminations could lead to changes in the actual workfunction and, therefore, give the appearance of different $\beta$ values. In our case, the RMS roughness of the diamond surfaces, as well as the metal films on diamond, was of the order of a few Å. We, therefore, do not expect the surface roughness to have a significant impact on the field electron measurements. Based on this consideration, a value of 1 has been assumed for $\beta$. The effective barrier heights $\varphi$ were obtained by fitting the field emission data to equation (3). Figure 12 shows this fitting of the field emission data for Cu on the hydrogen terminated surface. The fitted graphs exhibit different slopes which correspond to different distances

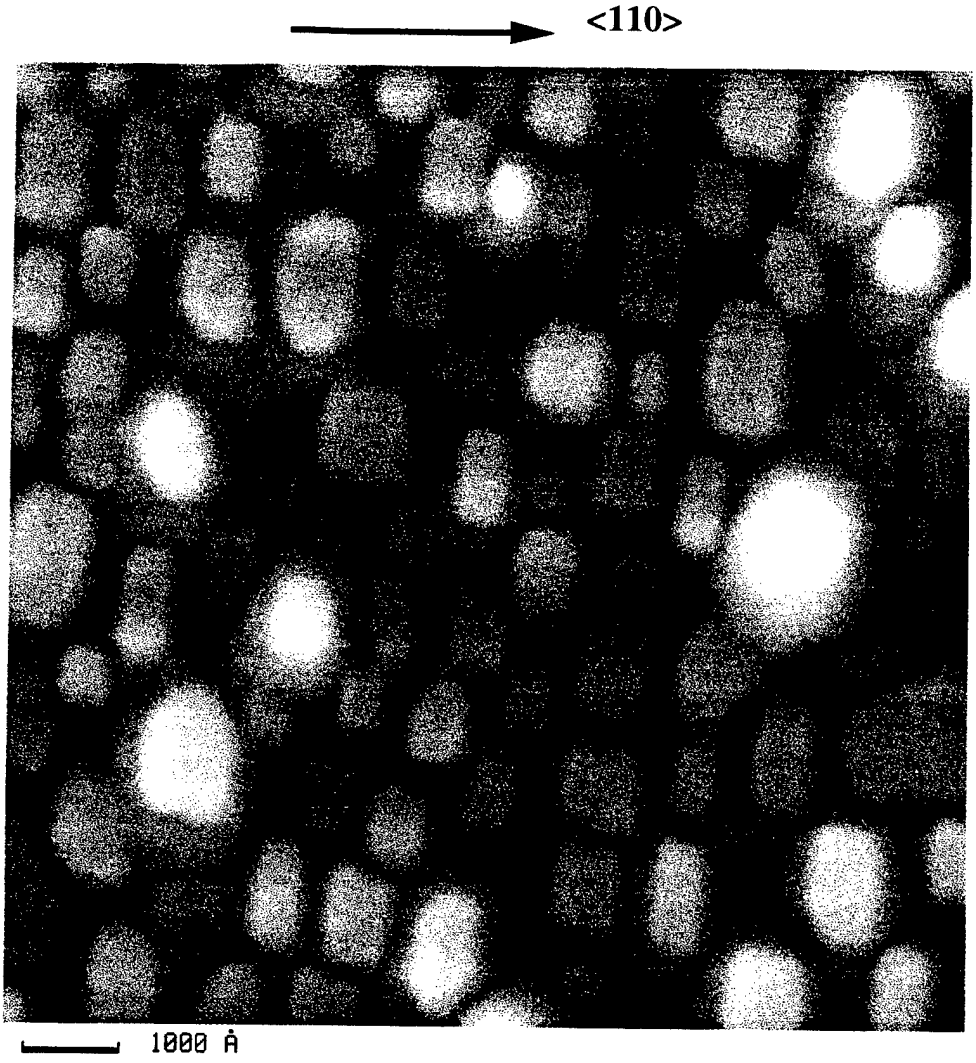


Figure 10b. Atomic force micrograph of 100 Å of Cu on diamond deposited at 500°C. Oriented islands of ~ 500–1000 Å in size are detected. The islands are oriented along the <110> directions of the underlying diamond (100) substrate.

between the anode and the sample. After correcting for the distance, the curves all resulted in about the same value for the effective barrier height. The values and the standard deviations are listed in Table II.

D. Discussion

From the UPS spectra of the diamond surfaces before copper deposition, different Fermi level positions were determined for the different surface terminations. Values between 0.3 eV and 0.4 eV were measured for $E_F - E_V$ for the clean or hydrogen terminated surfaces. This corresponds to the position of the boron impurities in the bandgap. And it did not appear to change for the (100), (111) and (110) surface orientations. A larger value of 1.0 eV for $E_F - E_V$ due to surface pinning was found for oxygen termination. After copper deposition the position of the Fermi level increased except for the clean (111) surface where no change has

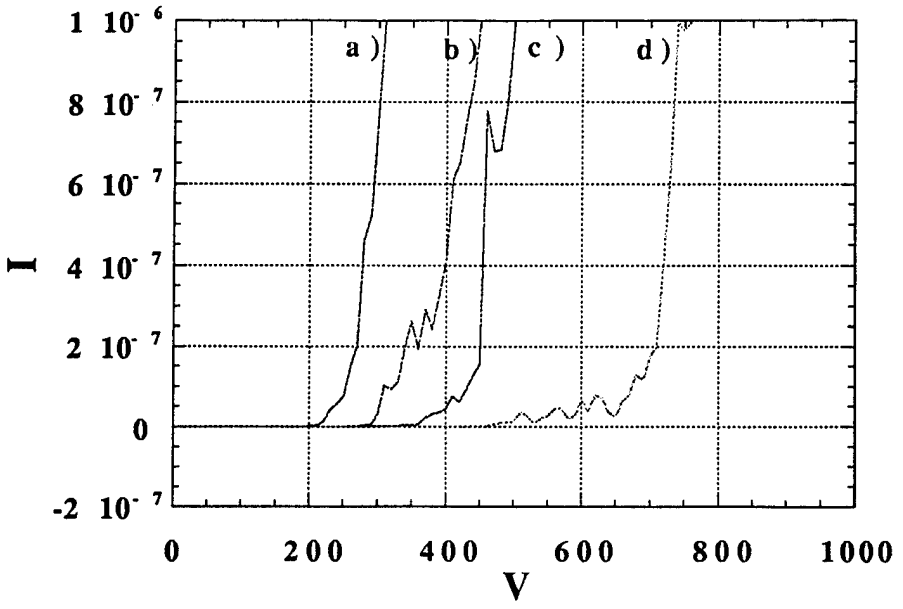


Figure 11. Field emission current–voltage curves for Cu on a hydrogen terminated type IIb single crystal diamond (100) sample. Distances between the sample and the anode: a) 5.4 μm, b) 8.8 μm, c) 13.2 μm, d) 26.4 μm.

Table II. Results of Electron Emission Measurements

| Sample UPS | | Field Emission Threshold (V/ μm) | Barrier Height (eV) |
|---|---|---|---|
| C(100) oxygen terminated | PEA, $\chi = 1.4$ eV | 79 ± 7 | 0.23 ± 0.01 |
| Cu/C(100) clean | NEA, $\chi < 0$, $\Phi_B = 0.70$ eV | 25 ± 3 | 0.10 ± 0.01 |
| Cu/C(100) hydrogen | NEA, $\chi < 0$, $\Phi_B = 0.90$ eV | 35 ± 4 | 0.15 ± 0.02 |
| Cu/C(100) oxygen | PEA, $\chi = 0.75$ eV, $\Phi_B = 1.60$ eV | 53 ± 4 | 0.21 ± 0.01 |

PEA: positive electron affinity, NEA: negative electron affinity. The error margins for $\chi$ and $\Phi_B$ from the UPS measurements are 0.1 eV. The averages and standard deviations of the field emission measurements at different distrances are shown as the field emission threshold and the barrier height. The threshold currrent is 0.1 μA.

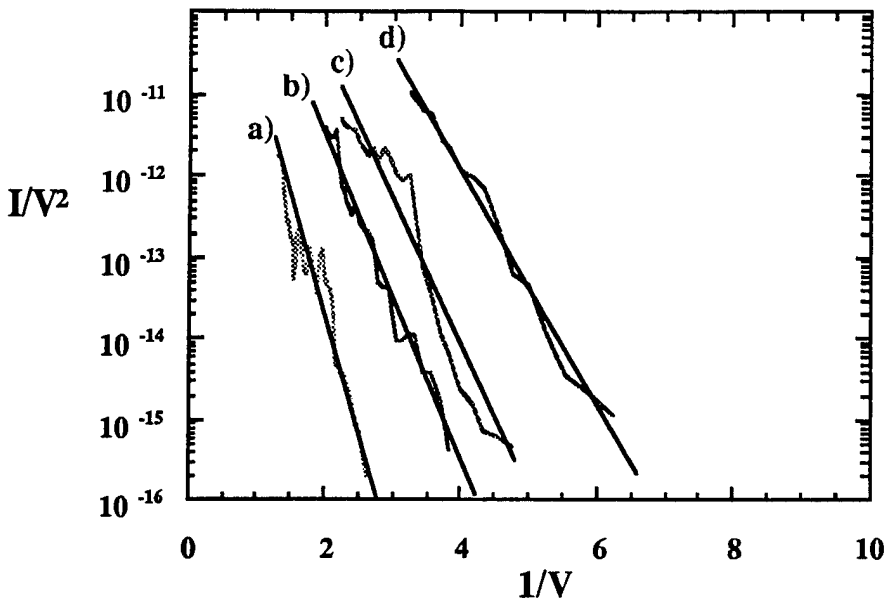


Figure 12. Fitting field emission current-voltage curves (for Cu on a hydrogen terminated type IIb single crystal diamond (100) sample) to Fowler Nordheim equation. Distances between the sample and the anode: a) 5.4 μm, b) 8.8 μm, c) 13.2 μm, d) 26.4 μm.

been found. The observed increase in $E_F - E_V$ corresponded to shifts to lower energies in the spectra of the same magnitude. The Schottky barrier height of copper on clean surfaces was determined to be about 0.2 eV to 0.3 eV smaller than for copper on hydrogen terminated surfaces with the same orientation, see Fig. 13.

The following equation is specific for photoemission of thin metal layers (less than the electron mean free path) on semiconductors. The model assumes that the structure can be characterized with two interfaces: vacuum-metal and metal-diamond. The effective electron affinity can then be expressed in terms of the metal workfunction and the Schottky barrier formed with a p-type semiconductor [34]:

$$\chi = (\Phi_M + \Phi_B) - E_G \qquad (3)$$

Using the bandgap of diamond $E_G$= 5.47 eV, the workfunction of Cu for the (100) surface $\Phi_M$ = 4.59 eV and the measured Schottky barrier height the electron affinity can be calculated. For the clean surface a value of -0.2 eV is obtained while 0 eV and 0.7 eV is obtained for the hydrogen and oxygen terminated surfaces, respectively. These results are consistent with observing a NEA for Cu on the clean (100) surface and a positive electron affinity of $\chi \cong 0.75$ eV for Cu on the surface covered with oxygen.

For the H terminated surface a NEA was detected. The question may be asked whether the observation reflects the properties of the Cu-diamond (100) interface or the initial

H-termination of the diamond (100) surface. Subsequent to deposition of 10 Å of Cu the NEA peak was still measured, and the width of the spectra was reduced by ~ 0.4 eV. This spectral change is inconsistent with a superposition of the substrate H induced NEA and the spectra of the Cu layer. We, therefore, suggest that the Cu-diamond (100) interface itself exhibits a NEA. The calculated value of $\chi \equiv 0$ eV is still in essential agreement with measuring a NEA after Cu deposition.

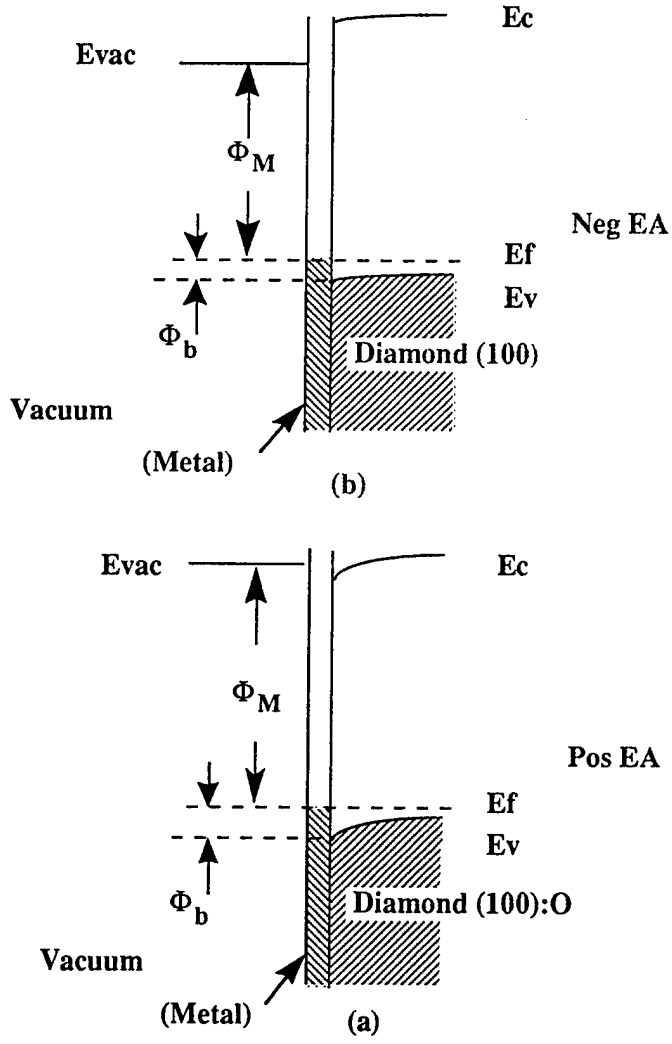


Figure 13. Band diagrams of the copper-diamond interface. For copper on the oxygen terminated surface (a) the sum of the Schottky barrier height and work function for metal on diamond is greater than the band gap of diamond resulting in a positive electron affinity. For copper on the clean or hydrogenated surface (b) the Schottky barrier height added to the metal work function is less than the diamond bandgap. This corresponds to a NEA.

Applying this model to Cu on the (111) surface and assuming a workfunction of $\Phi_M$ = 4.94 eV, we calculate values of $\chi \cong$ - 0.2 eV and $\chi \cong$ 0 eV for the clean and H terminated surface, respectively. Similar to the (100) surface this is in agreement with observing a NEA for the clean surface. It may also be consistent with measuring a NEA for the surface covered with hydrogen. In the same manner using the workfunction of Cu $\Phi_M$ = 4.48 eV for the (110) surface, electron affinities of $\chi \cong$ - 0.4 eV for Cu on clean and $\chi \cong$ - 0.1 eV for Cu deposited on H terminated samples. Both values are consistent with the experimentally observed NEA from these surfaces. These values for the electron affinity are summarized in Table I.

Also, it has been reported that carbon contamination can lower the workfunction of Ni [35]. The first layer of Ni deposited on diamond may have a different workfunction due to the carbon of the diamond. This effect may also occur for Cu on diamond, but such an effect would only lead to a larger calculated reduction of the electron affinity for Cu on the clean and H terminated surfaces. This would be consistent with our results. For Cu on the oxygen terminated surface the measured and calculated values for the electron affinity are consistent with each other. Thus, at least for the latter case this effect is not expected to be significant.

Previously, Eq. 3 has been used successfully to relate the electron affinity and Schottky barrier of Ti, Ni, Co, Cu and Zr deposited on diamond [11-18]. In these studies it has been found that the Schottky barrier height for clean surfaces was lower than for surfaces terminated by oxygen or hydrogen. Indeed, metal-diamond interfaces exhibiting a NEA have a lower Schottky barrier height than those exhibiting a positive electron affinity. Surface preparation apparently has a significant impact on the properties of the interface subsequent to metal deposition [11-18]. For Ni deposited on clean (111) surfaces a NEA has been observed [12]. In comparison for Ni on H terminated (111) surfaces a positive electron affinity and a larger Schottky barrier height were measured. Erwin and Pickett [36-39] and Pickett, Pederson and Erwin [40] calculated a Schottky barrier height of less than 0.1 eV for the most stable configuration for Ni on clean (100) and (111) surfaces. A theoretical study of Cu on the (111) surface by Lambrecht [19] considered different interface structures. For the clean surface the tetrahedral position for the Cu atoms was found to be most favorable energetically. This structure led to a Schottky barrier height of less than 0.1 eV. In comparison, for the in-hollow position a Schottky barrier of ~ 0.5 ± 0.2 eV was calculated. These results indicate a strong dependence of the Schottky barriers on the actual interface formation. The formation energies are somewhat different with 2.3 ± 0.5 J/m2 for the tetrahedral structure and 3.8 ± 0.5 J/m2 for the in-hollow position. Taking these uncertainties into account the values for the formation energies may be quite similar. The value of 0.3 eV for the Schottky barrier of Cu on the clean diamond (111) surface measured in our study does fall between the values for the two

geometries considered in the calculations, and it may be suggested that both geometries actually form at the interface.

For Cu on the H terminated (111) surface Lambrecht calculated a Schottky barrier of greater than 1.0 eV. This value is considerably larger than the measured value of 0.5 eV from our experiments. The Schottky barrier measured for Cu on the H terminated surface is, however, larger than the value measured for the clean (111) surface. One explanation may be that the Cu-diamond interface was not completely H saturated. Portions of the interface could be adsorbate free. Therefore, the measured Schottky barrier would be an average of the values from different interface structures. We did, however, observe a NEA following the H plasma clean, and it is questionable whether significant portions of the (111) surface would remain adsorbate free after a H plasma exposure. It is also possible that H may have been displaced from the interface during the Cu deposition.

Overall for the (100), (111) and (110) surfaces the Schottky barrier increases from the clean surface to the H terminated surface. For the oxygen terminated (100) surface an even greater Schottky barrier has been measured, and the value of the electron affinity is correlated with the Schottky barrier. Metal–diamond interfaces exhibiting a lower Schottky barrier also exhibit a lower electron affinity. The surface termination of the diamond substrate before metal deposition is important for determining the properties of the metal–diamond interface. In order to obtain a minimum for the Schottky barrier and the electron affinity, a surface treatment removing surface chemisorbed species is necessary.

In a previous study of Ti on diamond, it has been found that the metal induced NEA peak was significantly reduced once the uniform metal film reached several Å in thickness. In particular, the intensity was reduced by about 50% for an increase in the thickness of the Ti layer from 2Å to 3Å [11]. Only electrons from within a few scattering lengths of the surface will get emitted into vacuum and can be detected. In our study, we have determined reductions by about 10% for an increase in the Cu thickness from 2Å to 3Å. We have also observed island formation for the Cu layers by AFM. This is consistent with a NEA peak still being more pronounced for thicker Cu films than for the case of uniform Ti layers.

For 1Å of Cu deposited onto clean surfaces at room temperature strong NEA type emission could be clearly observed. However, 1Å of Cu deposited onto a clean surface at 500°C resulted in only very little intensity at the position of the conduction band minimum. Only after 2Å of Cu was a clear NEA feature detected. This can be correlated with the stronger tendency of islanding for deposition of up to 2 Å of Cu at 500°C, as observed by AFM. For 1Å of Cu deposited at 500°C only a few islands would be expected to form. Also, if the center regions of the islands were thicker than the electron mean free path ( $\leq$ 5 Å), electrons originating from the copper-diamond interface could not get emitted. Then, only NEA effects from around the edges of the islands could be detected. This would result in NEA emission from only a small

fraction of the surface area. This is consistent with the very weak NEA emission observed by UPS. For further Cu deposition a larger number of islands would be formed. This would be expected to lead to an increase in the NEA emission intensity. For Cu deposited on clean diamond substrates at room temperature no island formation has been detected up to 2Å. This would correspond to a larger part of the surface area exhibiting a NEA for 1Å of Cu. For more than 2Å of Cu a large number of islands were observed, and again NEA emission would occur from a significant part of the surface. These considerations are in agreement with our observations from the UPS spectra.

We have found that a few Å thick Cu films deposited on diamond at room temperature exhibit LEED patterns corresponding to the orientation of the underlying surface. For thicker Cu layers (40Å) the diffraction patterns faded. The first few monolayers of Cu on the different diamond surfaces are apparently epitaxial. This could be correlated with the FCC lattice structure of Cu and the close lattice match with diamond. In comparison, for Cu deposited while the substrates were held at 500°C resulted in LEED patterns even for the thickest films grown (100Å, 2000Å [10]). By means of AFM scans of thick Cu films (100Å, 2000Å [10]) showing islands oriented with respect to the underlying diamond substrates, as well as Rutherford backscattering experiments [10] it was confirmed that the Cu films grew epitaxial.

It is significant that the copper on diamond samples with a NEA retained this characteristic following air exposure. The air stability may be important for the development of cold cathode devices stable in a technical vacuum and may also simplify their production process.

According to the field emission threshold results, deposition of Cu onto the clean, hydrogen and oxygen terminated diamond (100) surfaces improves the emission properties. The best results were obtained for Cu on the clean surface. The experiments presented here were on similarly prepared natural diamond surfaces with a low surface roughness particularly as compared to diamond films. The roughness of the surfaces before and after metal deposition was comparable and of the order of a few Å. The field enhancement factor, $\beta$, may not be expected to be significantly different for the various surfaces considered. The field electron emission process is more complicated than photoemission since it includes contributions from electron injection at the back interface, conduction through the bulk, and finally emission into vacuum. The last step may be the same for both photo- and field emission. Because of the added complexity, it is often difficult to attribute changes in the effective barrier height to specific differences in the samples. While field emission is often described by the Fowler-Nordheim expression, it should be noted that this expression was derived for emission from metal surfaces, assuming no field inside the bulk of the material. An equation for microscopic dielectric regions has been proposed [41], but this approach would not be a reasonable model for our case with a diamond substrate thickness of 0.25 mm.

Bandis and Pate [42] have performed simultaneous field emission and photoemission measurements from (111) 1×1:H natural p - type diamond to determine the origin of the field emitted electrons. This surface exhibited a NEA which allowed the determination of the position of the conduction band minimum. They report that the electrons due to field emission originate from the valence band maximum.

The diamond samples used in our study were p-type also. Electrons that originate from the conduction band minimum can freely leave a NEA surface. This is the case for electrons detected in UPS measurements. From our results we expect the energy of the vacuum level for Cu on clean and H terminated surfaces to be near the conduction band of the diamond. Then even for a small NEA, the field emitted electrons would have to overcome a significant barrier at the surface to be emitted into vacuum, assuming that they came from the valence band maximum. Inducing a NEA on a positive electron affinity diamond surface would then reduce the surface energy barrier but not entirely remove it for field emitted electrons. The actual reduction of this surface barrier may still have a significant impact on the field emission results. Considering the case of depositing copper onto an oxygen terminated diamond surface, the lowering of the field emission threshold from 79 V/μm to 53 V/μm may be attributed to the measured reduction of the electron affinity from 1.4 eV for an oxygen terminated surface to 0.75 eV for Cu on this surface. Deposition of copper onto a clean or a hydrogen terminated diamond surface results in even lower values for the field emission threshold. This may be due to lower values for the electron affinity. The threshold value is the smallest for copper on clean diamond surfaces. And for this case the NEA is expected to be the most negative, as calculated from the Schottky barrier height (see Table I). This is consistent with the correlation of the lowering of the field emission threshold with the reduction in electron affinity and correspondingly in surface energy barrier height.

Both the UPS and field emission measurements show consistent trends for Cu on the clean, H and O terminated surfaces. The lowest Schottky barrier heights and lowest electron affinities have been found for Cu on the clean surfaces. The same is the case for the lowest field emission threshold fields. Whereas interfacial hydrogen or oxygen caused all these values to increase. The barrier for field emission is, however, expected to be near the bandgap value of the diamond while significantly lower values were deduced from the field emission. This substantial difference may be an indication that

## E. Conclusions

In this study, UV photoemission and field emission have been employed to characterize the copper-diamond (100), (111) and (110) interfaces. The lowest values for the Schottky barrier height were obtained for copper deposited on adsorbate free surfaces. Hydrogen at the interface led to an increase in Schottky barrier height. The highest value of the Schottky barrier was

obtained for an oxygen terminated surface. The measured values were consistent with a theoretical model for Cu on the clean and hydrogen terminated (100) surface. A NEA was detected for thin layers of copper deposited on clean and H terminated surfaces. The NEA was found to be stable in air. A lower Schottky barrier height generally leads to a lower electron affinity. The results were consistent with a model that in which the Cu–diamond structure was described in terms of the measured Schottky barrier and the Cu workfunction appropriate to the surface. From the field emission measurements it was observed that metal deposition tends to lower the threshold field compared to the oxygen terminated diamond surface. The lowest value was measured for Cu on the clean diamond surface. Surface cleaning of the diamond samples before metal deposition is therefore suggested to be critical in determining the Schottky barrier height and thus the electron emission properties.

F. Acknowledgements

This work has been supported in part by the Office of Naval Research (Contract No. N00014-92-J-1477).

G. References

1. F.J. Himpsel, J.A. Knapp, J.A. van Vechten, D.E. Eastman, Phys. Rev. B 20, 624 (1979).
2. C.A. Mead and T.C. McGill, Phys. Lett. **58A**, 149 (1976).
3. F.J. Himpsel, D.E. Eastman and J.F. van der Veen, J. Vac. Sci. Technol. **17**, 1085 (1980).
4. J.W. Glesener, A.A. Morrish and K.A. Snail, J. Appl. Phys. **70**, 5144 (1991).
5. M.W. Geis, D.D. Rathman, D.J. Ehrlich, R.A. Murphy and W.T. Lindley, IEEE Electron Device Lett. **8**, 341 (1987).
6. H. Shiomi, H. Nakahata, T. Imai, Y. Nishibayashi and N. Fujimori, Jpn. J. Appl. Phys. **28**, 758 (1989).
7. T. Tachibachi, B.E. Williams and J.T. Glass, Phys. Rev. B **45**, 11975 (1992).
8. M.C. Hicks, C.R. Wronski, S.A. Grot, G.S. Gildenblat, A.R. Badzian, T. Badzian and R. Messier, J. Appl. Phys. **65**, 2139 (1989).
9. S.A. Grot, S. Lee, G.S. Gildenblat, C.W. Hatfield, C.R. Wronski, A.R. Badzian, T. Badzian and R. Messier, J. Mater. Res. **5**, 2497 (1990).
10. P.K. Baumann, T.P. Humphreys, R.J. Nemanich, K. Ishibashi, N.R. Parikh, L.M. Porter and R.F. Davis, Proc. of the 4th European Conference on Diamond, Diamond-like and Related Materials, edited by P.K. Bachmann, I.M. Buckley-Golder, J.T. Glass, M. Kamo: J. Diamond Rel. Mat. **3**, 883 (1994).
11. J. van der Weide and R.J. Nemanich, J. Vac. Sci. Technol. B **10**, 1940 (1992).
12. J. van der Weide and R.J. Nemanich, Phys. Rev. B, **49**, 13629 (1994).
13. P.K. Baumann and R.J. Nemanich, Appl. Surf. Sci.**104/105**, 267 (1996).
14. P.K. Baumann and R.J. Nemanich, in *Diamond for Electronic Applications*, edited by C. Beetz, A. Collins, K. Das, D. Dreifus, T. Humphreys, P. Pehrsson, Mater. Res. Symp. Soc. Proc. **416** MRS, Pittsburgh, PA, 157 (1996).
15. P.K. Baumann, S.P. Bozeman, B.L. Ward and R.J. Nemanich, in *III-Nitride, SiC and Diamond Materials for Electronic Devices*, edited by D.K. Gaskill, C. Brandt, R.J. Nemanich: Mater. Res. Symp. Soc. Proc. **423**, MRS, Pittsburgh, PA, 143 (1996).
16. P.K. Baumann, S.P. Bozeman, B.L. Ward and R.J. Nemanich, "Characterization of

Metal - Diamond Interfaces": Proceedings of DIAMOND '96, the 7th European Conf. on Diamond, Diamond-like and Related Materials jointly with ICNDST-5, the 5th International Conf. on the New Diamond Science and Technology, edited by J.C. Angus, P.K. Bachmann, I.M. Buckley-Golder, O. Fukunaga, J.T. Glass, M. Kamo: J. Diamond Rel. Mat. **6**, 398 (1997).

17. P.K. Baumann and R.J. Nemanich, "Electron Affinity and Schottky Barrier Height of Metal - Diamond Interfaces": Proceedings of PCSI - 24, the 24th Conf. on Physics and Chemistry of Semiconductor Interfaces: J. Vac. Sci. Technol. B **15(4)** (1997) accepted for publication.
18. P.K. Baumann and R.J. Nemanich, J. Appl. Phys., submitted for publication.
19. W.R.L. Lambrecht, Physica B **185**, 512 (1993).
20. M. Marchywka, P.E. Pehrsson, S.C. Binari and D. Moses, J. Electrochem. Soc., **140**, No. 2, L19 (1993).
21. P.K. Baumann, T.P. Humphreys and R.J. Nemanich, in *Diamond, SiC and Nitride Wide Bandgap Semiconductors*, edited by C.H. Carter, G. Gildenblat, S. Nakamura, R.J. Nemanich, Mater. Res. Soc. Proc. **339**, Pittsburgh, PA, 69 (1994).
22. T.P. Schneider, J. Cho, Y.L. Chen, D.H.Mahler and R.J. Nemanich, in *Surface Chemical Cleaning and Passivation for Semiconductor Processing*, edited by G.S. Higashi, E.A. Irene, T. Ohmi Mater. Res. Soc. Proc. **315**, Pittsburgh, PA, 197 (1993).
23. B.B. Pate, Surf. Sci. 165, 83 (1986).
24. M.H. Hecht, J. Vac. Sci. Techno. B **8**, 1018 (1990).
25. C.Bandis, B.B. Pate, Surf. Sci. Let. **345**, L23 - L 27 (1996).
26. J. van der Weide and R.J. Nemanich, Appl. Phys. Lett. **62**, 1878 (1993).
27. J. van der Weide, Z. Zhang, P.K. Baumann, M.G. Wensell, J. Bernholc and R.J. Nemanich, Phys. Rev. B **50**, 5803 (1994).
28. B.B. Pate, in *Diamond: Electronic Properties and Applications*, edited by L.S. Pan, D.R. Kania, 35 (1995).
29. P.K. Baumann and R.J. Nemanich, Proc. of the 5th European Conference on Diamond, Diamond-like and Related Materials, edited by P.K. Bachmann, I.M. Buckley-Golder, J.T. Glass, M. Kamo: J. Diamond Rel. Mat., **4**, 802 (1995).
30. P.K. Baumann and R.J. Nemanich, J. Appl. Phys., submitted for publication.
31. W. Zhu, G.P Kockanski, S. Jin and L. Siebels, J. of Appl. Phys. **78**, 2707 (1995).
32. S.P. Bozeman, P.K. Baumann, B.L. Ward, M.J. Powers, J.J Cuomo, R.J. Nemanich and D.L Dreifus, Proc. of the 6th European Conference on Diamond, Diamond-like and Related Materials, edited by P.K. Bachmann, I.M. Buckley-Golder, J.T. Glass, M. Kamo: J. Diamond Rel. Mat. **5**, 802 (1996).
33. R. Gomer, *Field Emission and Field Ionization*, Cambridge, MA, (1961).
34. E.H. Rhoderick and R.H. Williams, *Metal-Semiconductor Contacts*, Clarendon, Oxford, (1988).
35. C. Weiser, Surf. Sci. **20**, 143 (1970).
36. S.C. Erwin and W.E. Pickett, Surf. Coat. Technol. **47**, 487 (1991).
37. S.C. Erwin and W.E. Pickett, Solid State Commun. **81**, 891 (1992).
38. W.E. Pickett and S.C. Erwin, Phys. Rev. B **41**, 756 (1990).
39. W.E. Pickett and S.C. Erwin, Superlatt. Microsruct. **7**, 335 (1990).
40. W.E. Pickett, M.R. Pederson and S.C. Erwin, Mater. Sci. Eng. B **14**, 87 (1992).
41. R.V. Latham, Vacuum **32** (3), 137 (1982).
42. C. Bandis, B.B. Pate, Appl. Phys. Lett. **69**, 366 (1996).

# IV. Distribution List

| | |
|---|---|
| Dr. Colin Wood<br>Office of Naval Research<br>Electronics Division, Code: 312<br>Ballston Tower One<br>800 N. Quincy Street<br>Arlington, VA 22217-5660 | 3 |
| Administrative Contracting Officer<br>Office of Naval Research<br>Atlanta Regional Office<br>100 Alabama Street, Suite 4R15<br>Atlanta, GA 30303 | 1 |
| Director, Naval Research Laboratory<br>ATTN: Code 2627<br>Washington, DC 20375 | 1 |
| Defense Technical Information Center<br>8725 John J. Kingman Road, Suite 0944<br>Ft. Belvoir, VA 22060-6218 | 2 |